8-1-2014

Characterization of Impulse Noise and Hazard Analysis of Impulse Noise Induced Hearing Loss using AHAAH Modeling

Qing Wu
Southern Illinois University Carbondale, qing2012@siu.edu

CHARACTERIZATION OF IMPULSE NOISE AND HAZARD ANALYSIS OF IMPULSE NOISE INDUCED HEARING LOSS USING AHAAH MODELING

by

Qing Wu

B.S., Southwest University of Science & Technology, 2004
M.S., Florida International University, 2008
M.S., Beihang University, 2009

A Thesis
Submitted in Partial Fulfillment of the Requirements for the
Master of Science

Department of Electrical & Computer Engineering
in the Graduate School of
Southern Illinois University Carbondale
August 2014

THESIS APPROVAL

CHARACTERIZATION OF IMPULSE NOISE AND HAZARD ANALYSIS OF IMPULSE NOISE INDUCED HEARING LOSS USING AHAAH MODELING

By

Qing Wu

A Thesis Submitted in Partial

Fulfillment of the Requirements

for the Degree of

Master

in the field of Electrical & Computer Engineering

Approved by:

Dr. Qin Jun, Chair

Dr. Lalit Gupta

Dr. Haibo Wang

Graduate School
Southern Illinois University Carbondale
3rd December 2014

AN ABSTRACT OF THE THESIS OF

Qing Wu, for the Master of Science degree in Electrical & Computer Engineering, presented on 3rd December 2013, at Southern Illinois University Carbondale.

TITLE: CHARACTERIZATION OF IMPULSE NOISE AND HAZARD ANALYSIS OF IMPULSE NOISE INDUCED HEARING LOSS USING AHAAH MODELING

MAJOR PROFESSOR: Dr. Qin Jun

Millions of people across the world are suffering from noise induced hearing loss (NIHL), especially under working conditions of either Gaussian noise or non-Gaussian noise that might affect human's hearing function. Impulse noise is a typical non-Gaussian noise exposure in military and industry, and generates severe hearing loss problem. This study mainly focuses on characterization of impulse noise using digital signal analysis method and prediction of the auditory hazard of impulse noise induced hearing loss by the Auditory Hazard Assessment Algorithm for Humans (AHAAH) modeling. A digital noise exposure system was developed to produce impulse noises with peak sound pressure level (SPL) up to *160* dB. The characterization of impulse noise generated by the system has been investigated and analyzed in both time and frequency domains. Furthermore, the effects of key parameters of impulse noise on auditory risk unit (ARU) are investigated using both simulated and experimental measured impulse noise signals in the AHAAH model. The results showed that the ARUs increased monotonically with the peak pressure (both P^+ and P^-) increasing. With increasing of the time duration, the ARUs increased first and then decreased, and the peak of ARUs appeared at about $t = 0.2$ ms (for both t^+ and t^-). In addition, the auditory hazard of experimental measured impulse noises signals demonstrated a monotonically increasing relationship between ARUs and system voltages.

Keywords: auditory hazard assessment algorithm for humans (AHAAH), auditory hazard prediction, auditory risk unit (ARU), digital noise-exposure system, frequency domain kurtosis (FDK), impulse noise, kurtosis, noise induced hearing loss (NIHL).

ACKNOWLEDGEMENTS

I would like to deliver so many thanks for people and their goodness in the Department of Electrical and Computer Engineering at Southern-Illinois University Carbondale (SIUC). Their support and guidelines help me to complete this study.

Firstly, I would like to thank my advisor Dr. Jun Qin for his professional advices and great understanding to this study.

Next I would like to thank my committee members Dr. Lalit Gupta and Dr. Haibo Wang of the Electrical and Computer Engineering Department at SIUC, for their expertise and kindness suggestions.

I am grateful for the help of Adam Johnston and Adam Wayne Schlag as their previous works on a noise-exposure system. I also want to appreciate my friends, Pengfei Sun, Kelly Wepsiec, and many other students. With their help and encouragement, I felt comfort and joy for my time in SIU.

Lastly, I would like to bring my personal thanks to brothers and sisters in church, my parents, and my husband Shiyu Xu, for their unchangeable love and care.

TABLE OF CONTENTS

LIST OF TABLES

TABLE PAGE

LIST OF FIGURES

FIGURE PAGE

CHAPTER 1

INTRODUCTION

1.1 Clinical motivation

Noise induced hearing loss (NIHL) has been ascribed to unexpected noise exposures, or unaware-frequently sounds either as Gaussian noises or non-Gaussian noises. Usually, NIHL occurs across industry and military fields. It affects human's hearing and might result in permanent hearing loss (Levey, Fligor, Ginocchi, & Kagimbi, 2012). According to recent survey, more than *10%* world's population has some sorts of hearing impairment (Hu, Sang, Lutman, & Bleeck, 2011). It is estimated that about *30* million Americans currently have some types of hearing loss due to daily noise exposures in their jobs (Daniel, 2007; Agrawal, Platz, & Niparko, 2008).

Human's hearing range mainly varies from *20* Hz to *20* KHz, which is defined by the standard sound pressure (SSP) transmission in air from *20* μPa to *20* MPa, or *0* dB Sound Pressure Level (SPL) to *240* dB SPL. Clinical evidences indicate that acoustic damages first occur inside human's cochlea, where the organ responses for high-frequency (HF) sound waves (Peter, Silaski, Wilmington, & Gordon, 2012). Whereas, impulse noise is such kind of noise that composes of high peak pressure in an extreme short time. Its high peak pressures could permanently damage the hearing cells, and potentially result in hearing loss in a specific frequency range of sound waves (Guinan & Peake, 1967) (Price & Kalb, 1986). Therefore, impulse noise is a critical issue in NIHL.

Traditional signal analysis tools, such as Fast Fourier transformation (FFT) (Hu, Sang, Lutman, & Bleeck, 2011), digital filters and so on, have been used to specify the characteristics of different types of noises in both time domain and frequency domain, in order to provide efficient noise metrics in NIHL (Zhu, Kim, & Song, 2009). Several auditory damage risk criterions (DRCs) have been investigated. Some have been applied as industry regulations and military standards (Chan P. C., Ho, Stuhmiller, & Mayorga, 2001). A mathematical model of noise hazard, Auditory Hazard Assessment Algorithm for Humans (AHAAH), has been proved previously to be correlated very highly with hearing loss to *50* Friedlander impulses from two sources at *5* different peak pressures (*135* dB to *145* dB) (Price & Kalb, 1991). AHAAH model is able to predict auditory hazard produced by impulse noises. It presents high prediction accuracy on a theoretical modeling for human auditory system, and finally has been implemented by an electro-acoustic model (Price, 2007).

This thesis focuses to characteristic impulse noise, to evaluate its key parameters, and to use auditory risk unit (ARU) for prediction of hazardous analysis in AHAAH model. Simulated sine wave signals and data generated from the noise-exposure system are both evaluated by metrics defined both in time domain and frequency domain.

1.2 Principle of noise induced hearing loss (NIHL)

1.2.1 Insights to human ear

To understand sound wave propagation in air and its effects to human ear is to necessarily discuss the anatomy and physiology of human ear. The insights to human ear will

simply explain how the ear receives sound and transmits the data to brain for decoding information. Human ear can be divided into three parts, the outer ear, the middle ear and the inner ear. Sound wave transmission is generally modeled as a mechanical wave that vibrates with frequencies and propagates through mediums as following processes.

Firstly, the acoustic wave propagates by collides of particles in air and enters into outer ear by repeating pattern of high pressure and low pressure regions moving through mediums (Gardner & Hawley, 1972). Theoretically, the external ear can be considered as a hard-walled tube with one close end, and it can amplify the acoustic pressure up to 10 dB (Gardner & Hawley, 1972). Whereas, an impulse noise with frequency over 4 kHz may damage human's hearing because of the amplification function of external ear (Gardner & Hawley, 1972). The external auditory canal is shaped in order to capture and direct the sound waves into the middle ear.

In the middle ear, sound wave propagation leads to mechanical vibrations by motions that the stapes repeatedly hit the eardrum. The sound wave transmits from middle ear into inner ear is also modeled as the sound wave energy transfers from air to fluid. Because such impedance matching between the middle ear and the inner ear, the sound wave is compressed from vibrations into pressures.

Inside the inner ear, the cochlea is a two-chambered, fluid-filled box with rigid side walls. Usually, the mechanics of cochlea is regarded as signal receivers. The sound wave propagates along the basilar membrane, which is covered by hair cells as pressure-signal receivers (Bekesy, 1953). Basic analysis method of cochlea is to pull the snail-shelled cavity as a long strip, shown as in Figure 1.The oval window, which the final ear bone is attached to, causes

the sound to travel down till the round window. Hence, while most of the pressures travel through the duct of the cochlea, the hair cells along the cochlea receive signals with different frequencies.

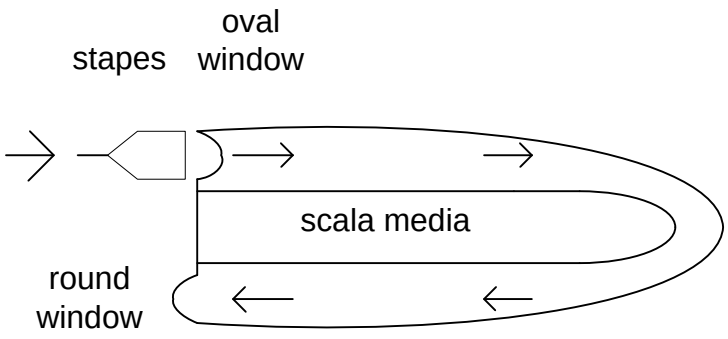

Figure 1 Long strip model of the inner ear

1.2.2 Different types and features of Noise induced hearing loss (NIHL)

Generally speaking, while DRCs present the capability of noise amount to create damages, emergence of NIHL can be divided into two phases, Temporary Threshold Shift (TTS) and Permanent Threshold Shift (PTS) (Melnick, 1991).

TTS is characterized as slight hearing loss within a recovery time due to ear fatigue but no damage to the sensory cells, for example, listening to loud music. This recovery time can take up to 48 hours, depending on the durations of different noise exposures. Several TTS experiments show that TTS reaches an asymptote after about 8 hour of noise exposure (Melnick, 1991). After frequent exposures to noise that is capable of producing TTS, the Permanent Threshold Shift (PTS) might occur. PTS is defined as the noise level, which will never recover

from TTS (Ward, 1991). Statistic data shows that a number of after-war soldiers are undergoing a PTS in NIHL, although the regulations of noise exposure level for weapon manufactory and proper hearing protection devices, for example, earplugs and earmuffs, might prevent such hearing loss in advance (Johnston A. M., 2011).

Measuring the hearing threshold shift and the amount of hair cell loss is widely used in acoustic traumatic under excessive exposure of sound levels (Roberto, Hamernik, Salvi, Henderson, & Milone, 1984). Noise exposure experiments on chinchilla were designed to test percentage of cell loss after excessive exposures to noise source, in order to define and differentiate TTS from PTS in NIHL (Clark, 1991). Some high frequency level noises cause vasoconstriction of the vessels in cochlea blood supply, which is the render to hair cell. Hair cell may be affected because of its anoxic (Alberti, 1997). The statistics of hair cell also presents the capabilities of acoustic signal receivers in cochlea, some typical noises directly damage hair cells during the sound wave transduction and may result in PTS. Therefore, NIHL focuses on hostile acoustic environment and specifies different prevention standards according to noise types.

1.3 Current hazard criterions for impulse noise analysis

1.3.1 Concept of impulse noise

Impulse noise is a category of acoustic noise with high peak pressure in a short time. It is mainly caused by sudden pressure changes or collisions. An impulse noise typically harms hair cells inside human inner ear with high amplitude, and may cause damages to the organ of corti in a short period (Kardous, Willson, & Murphy, 2005).

In this paper, the impulse noise also refers to the A-duration impulse noise, which is used to characterize the typical impulse noise generated by a military weapon (Johnston M. A., 2011). As shown in Figure 2, the typical A-duration impulse noise signal is shaped in high peak and followed an exponential decay. Friedlander (1946) suggested the characteristics of A-type impulse (Amrein, 2010) noise by an equation as below,

$$p(t) = P_s e^{-\frac{t}{t^+}}(1 - \frac{t}{t^+}) , \quad (1)$$

where *p(t)* is the pressure as a function of the time *t*, P_s is the peak pressure, and t^+ is the positive duration (Dewey, 2004).

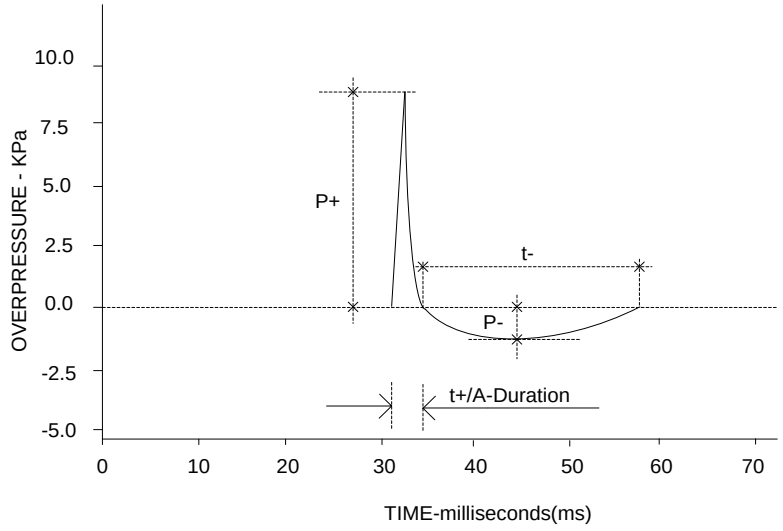

Figure 2 Demonstration for an A-Duration impulse waveform

1.3.2 Damage Risk Criteria (DRC) of impulse noise

A number of DRCs of impulse noise have been published, such as equivalent energy hypothesis (EEH), MIL-STD-1474D, and AHAAH model-based DRC. Basically, these DRCs can be divided into energy-based criteria and model-based criteria as below.

Atherley and Martin (Atherley & Martin, 1971) proposed A-weighted acoustic energy criterion in 1971. Patterson and Johnson developed the energy theory in 1994. Then Dancer et al. published the A-weighted acoustic energy criterion in 1995, known as L_{Aeq} criterion. Pfander (Pfander, Fongartz, & Brinkmann, 1980) and Smoorenburg (Smoorenburg, 1983) proposed the CHABA criteria, and developed it into military standards in 1997, known as MIL-STD-1474D. JAYCOR modification of the MIL-STD-1474D assumes that RACAL earmuff provide 15 dB additional protection by Chan et al. group in 2001 (Chan P. C., Ho, Stuhmiller, & Mayorga, 2001). In all, acoustic energy is widely used to assess the noise level. For example, United States Department of Labor proposes standards by using A-weighted sound levels and exposure time durations (U.S. Department of Labor).

Other than the energy-based DRCs, Price and Kalb published model-based DRC in 1991, AHAAH. It is a simulation model of a human full ear, called the electro-human ear. In the electrical model, the external ear functions as a signal amplifier, designed by a nonlinear transfer function and adjusted by parameters for ear protectors. Middle ear is modeled to simulate the transformation process of acoustic energy converting into mechanical energy. It is demonstrated that the external ear and middle ear effectively form a band pass filter elicited by the sound wave propagating coming from free field (Price & Kalb, 1991). In the inner ear, the cochlea is segmented to simulate longitudinally-varying impedance changes and also modeled as a time-frequency analyzer of wave propagation under such circumstances. Price uses AHAAH model to evaluate the risk by Auditory Risk Units (ARUs). In AHAAH model, it evaluates ARUs under

protection separately by the earmuff and ear plug, or non-protection situation, and it also offers evaluation in free field or indoor environment (Price, 1991).

1.4 Objectives of this study

The purpose of this study is to characterize impulse noise both in time domain and frequency domain. Experiments are based on both simulated impulse signals by Matlab and measured data by the noise-exposure system in SIU Medical Instrumentation Lab (MIB). The following works mainly apply digital signal processing (DSP) methods to evaluate the effects of key parameters of impulse noises, and analyze the auditory hazard predictions (i.e. ARU) in AHAAH model.

CHAPTER 2

THEORETICAL BACKGROUND

2.1 Characteristics of impulse noises

Equal energy hypothesis (EEH) is proposed based on the assumption that the risk of hearing loss produced by impulse noises will be monotonically increasing as the total A-weighted energy received by experimental target increases (Roberto, Hamernik, Salvi, Henderson, & Milone, 1984). EEH model also computes TTS and PTS to define the hearing damage degree, by using several features of noises, such as amplitude, time duration, and repetition cycle.

Moreover, AHAAH model defines a damage unit, ARU, to specify a permanent hearing loss as the threshold. For daily or near daily occupational exposures, the limit should be reduced to 200 ARUs (Binseel, Kalb, & Price, 2009).

2.1.1 EEH model

The definition of equivalent energy is a measuring method for impulse noise energy. Based on the conception of Sound Pressure Level (SPL), the instantaneous SPL can be described in decibels as below,

$$dB\ SPL = 20 \times log_{10}(\frac{p}{p_0})\ , \tag{2}$$

where the reference sound pressure p_0 as about 20 μ Pa.

The time-averaged squared sound pressure defines the equivalent continuous A-weighted sound pressure level, $L_{AEq,L}$. It is expressed as below,

$$L_{Aeq,L} = 10 \times log_{10}[\frac{1}{t_2-t_1} \times \int_{t_1}^{t_2} \frac{p_A^2(t)}{p_0^2} dt] \quad (3)$$

where t_2-t_1 is the period T over which the average is taken starting from t_1 and ending in t_2 (ISO, 1990-01-15).

The noise exposure level normalized to a nominal 8 hour working day, $L_{Aeq,8hr}$ indicates that the worker is kept in noise exposure by the same source without physically environment changes. It can be expressed as below,

$$L_{Aeq,8hr} = 10 \times log_{10}\left[\frac{1}{t_2-t_1} \times \int_{t_1}^{t_2} \frac{p_A^2(t)}{p_0^2} dt\right] + 10 \times log_{10}\frac{t_2-t_1}{T_{8hr}} + 10 \times log_{10}N, \quad (4)$$

where t_2-t_1 is the period T over which the average is taken starting from t_1 and ending in t_2, T_{8hr} is 28800 s, and N represents number of events. In this paper, we set N = 1 while the impulse noise is the only one source/event in this damage risk criterion (Murphy & Kardous, 2012).

2.1.2 Characteristics of impulse noise

Peak positive pressure (P^+) and peak negative pressure (P^-)

In order to analyze the amplitudes of the sound waves, the peak pressure is supposed to be as one of the key parameters to be calculated.

A duration (t^+) & negative time duration (t^-)

As discussed in chapter 2.2, A-duration wave has typical characteristics as Figure 2. We also define four key parameters of an impulse noise wave shown in table 1, including peak

positive pressure P^+, peak negative pressure P^-, time duration of the compressive wave t^+, and time duration of the tensile wave t^-.

Table 1 Definitions of key parameters of impulse noise

Name	Notation	Notes
p-positive	P^+	peak positive pressure in an impulse noise waveform (KPa)
p-negative	P^-	peak negative pressure in an impulse noise waveform (KPa)
t-positive	t^+	time duration of compressive wave (msec)/ A-duration
t-negative	t^-	time duration of tensile wave (msec)

Based on the definitions and notations of these parameters are listed in Table 1, the effects of four key parameters of an impulse noise in AHAAH model will be discussed in the following chapters.

Statistic Kurtosis

The fourth and the second moments are defined as below to calculate statistic kurtosis. Fourth moment m_4, second moment m_2, and the kurtosis β are defined respectively as below,

$$\mathrm{m}_4 = \frac{1}{N}\sum(x_i - \overline{\mathrm{x}})^4, \tag{5}$$

$$\mathrm{m}_2 = \frac{1}{N}\sum(x_i - \overline{\mathrm{x}})^2, \tag{6}$$

$$\beta = \frac{\mathrm{m}_4}{\mathrm{m}_2{}^2}. \tag{7}$$

In acoustic sound wave analysis, it is supposed that for a random variable *x*, where *x* represents the peak pressure for an instantaneous sound wave, and that the average value is about

zero in a long time evaluation. Combined to the mathematically concept of kurtosis, which is squared second moment divided by the fourth moment, fourth moment for acoustic wave acoustic_m_4, second moment for acoustic wave acoustic_m_2, the kurtosis equation for acoustic wave acoustic_β are defined respectively as below,

$$\text{acoustic\_}m_4 = \frac{1}{T}\int_0^{\mathrm{T}} \mathrm{p}^4(\mathrm{t})\mathrm{dt}\,, \tag{8}$$

$$\text{acoustic\_}m_2 = \frac{1}{T}\int_0^{\mathrm{T}} \mathrm{p}^2(\mathrm{t})\mathrm{dt}\,, \tag{9}$$

$$\text{acoustic\_}\beta = \frac{\text{acoustic\_m}_4}{\text{acoustic\_m}_2{}^2} \text{ (Erdreich, April 1986).} \tag{10}$$

Obviously, the time integral of squared pressure in kurtosis calculations varied because of different time domain. Consider a typical impulse sound wave collected in one time cycle, the definition of critical level will be grounded on the segmentation algorithm in a regional dose or specific time duration (Wang & Chen, Oct. 2009).

Hence, it is necessary to separate an impulse noise into small time durations to calculate the regional kurtosis as shown in Figure 3. And define the statistic kurtosis wave in time domain as follows,

$$\mathrm{K_j} = \frac{\frac{1}{\mathrm{T}}\int_0^{\mathrm{T}} \mathrm{p}^4(\mathrm{t})\mathrm{dt}}{\left(\frac{1}{\mathrm{T}}\int_0^{\mathrm{T}} \mathrm{p}^2(\mathrm{t})\mathrm{dt}\right)^2} = \frac{\mathrm{M}\times\sum_{\mathrm{i}=(\mathrm{j}-1)\times\mathrm{M}+1}^{\mathrm{j}\times\mathrm{M}} \mathrm{p_i^4(t)}}{\left(\sum_{\mathrm{i}=(\mathrm{j}-1)\times\mathrm{M}+1}^{\mathrm{j}\times\mathrm{M}} \mathrm{p_i^2(t)}\right)^2}\,, \tag{11}$$

where f_s is sampling frequency, T is for one cycle $T = M \times 1/fs$, and M stands for the number that T is divided into small regions.

Set M as a constant will bring a different view. For example, if we set M = 3, while we have an impulse wave intensities of 0, 1000, 0. The average will be about 330 and contributes to

the kurtosis value of 1.5186. However, if we took M = 3000, and we will see the average is 1 while kurtosis value will be about 3000. And this example is also easy to calculate in acoustic kurtosis to prove that M is one key parameter to be fixed in kurtosis calculation. Hence, the M should be just defined to cover the waveform as a unit or basic definition in this thesis.

$$K(t) = \max(K_j), \tag{12}$$

where statistic kurtosis in time domain $K(t)$ is selected as the max value to be cared in M segmentation time domain, where $t = M$ is set as 1.2 ms in this thesis. We approximate the max(K_j) appears from the first zero point before the peak pressure shown as below.

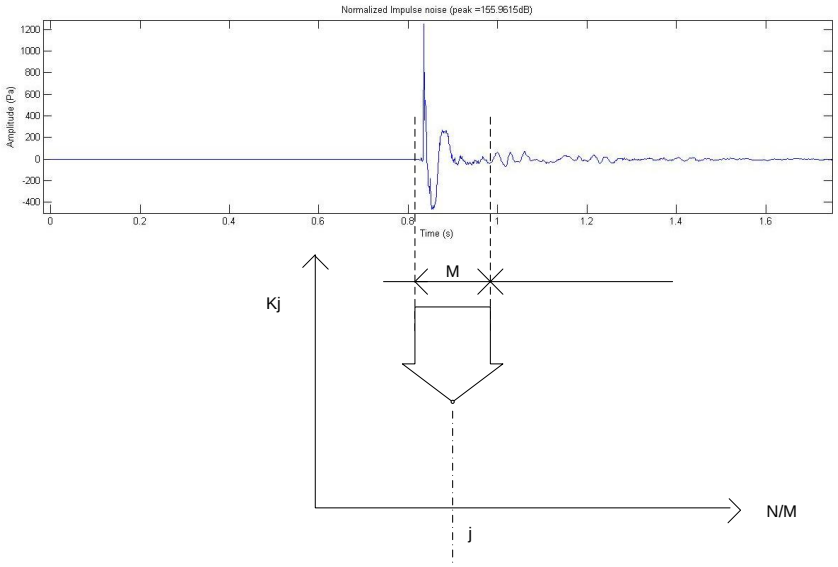

Figure 3 Illustration to definition for kurtosis wave in a fixed time domain M

2.2 Introduction to AHAAH model

The cochlea is a two-chambered, fluid-filled box with rigid side walls. The partition between the chambers is rigid; except for a tapered basilar membrane (BM) which becomes

progressively more compliant toward the apex (Price & Kalb, 1991). The AHAAH model reproduces the measured transfer functions from the free field to the stapes and translates stapes motion into BM displacements (Price, 2007). By the implementation of the system in electrical circuit, the active middle ear muscle contractions can be analyzed, which occurs in response to the sound or in advance of the arrival of the sound (Binseel, Kalb, & Price, 2009). Shown in Figure 4 as below, the electrical circuit is simulated under characteristic transfer functions of human ear behaviors.

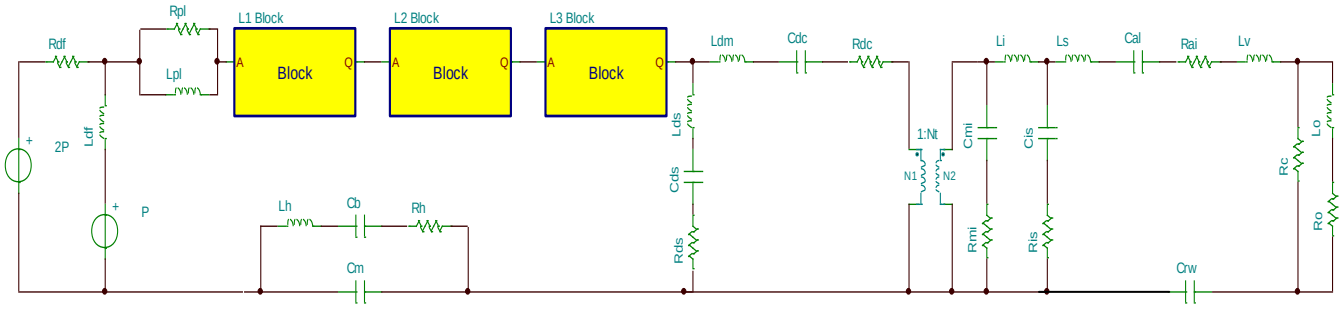

Figure 4 Schematic diagram of electrical circuit design for AHAAH model, from left to right, each block demonstrate human ear structure respectively, where *L1* block represents concha, *L2* and *L2* blocks represent the ear canal, circuit design details will demonstrate in the following chapters.

An evaluation of ARU is given as the terminal output of AHAAH that yield a prediction of immediate threshold shift, which in turn also provides a prediction of permanent threshold shift and hair cell loss (Price, 2007).

In this thesis, we used an unmodified AHAAH model to investigate the effects of key parameters of an impulse noise. The software of AHAAH model (beta release W93e) was downloaded from the website of United States Army Research Laboratory. All estimations of ARUs were calculated using “no protector, unwarned” setting in the AHAAH model.

2.2.1 External ear model of AHAAH

In AHAAH model, it approximates the diffraction-radiation combined sound field model as a spherical baffle, by which sound wave diffracts to the location of the ear canal (Price & Kalb, 1991). To realize the equivalent circuit, an imaginary tube and massless frictionless piston are first modeled to simulate the incoming plane wave from a free-field pressure microphone (Bauer, 1967). Consider human head as a solid sphere with radiu 'a_s' showed in Figure 5 (a), and the incoming acoustic plane wave (with pressure amplitude p) enters into ear canal through a tube model as Figure 5 (b). AHAAH suggests an exponential math model for external ear simulation as in Figure 5 (c), where the ear canal and the concha are modeled respectively as a cylindrical tube. Outer ear functions an amplifier for the incoming acoustic wave. The transfer function defines as the ratio of free-field sound pressure and the sound pressure of the concha entrace with related paramter table 2. Figure 5 (d) illustrates a 10-section network analog design for outer ear model (Gardner & Hawley, 1972), and Figure 5 (e) displays the voltage ratio of output and input versus frequency (Hz). Electrical design realizes the external ear model into a 16-section network analog design in AHAAH model.To compute the i_{th} component of equavalent capacitor and equavalent inductance in Figure 5 (f), is to use the volumn V_i of the exponential external ear model in Figure 5 (c) as below,

$$V_i = \begin{cases} \frac{S_1(e^{m(x_2-L_1)}-e^{m(x_1-L_1)})}{m}, & x_1 > L_1 \; and \; x_2 > L_1 \\ S_1(x_2-x_1), & x_1 < L_1 \; and \; x_2 < L_1 \\ S_1(L_1-x_1)+\frac{S_1(e^{m(x_2-L_1)}-1)}{m}, & x_1 < L_1 \; and \; x_2 > L_1 \end{cases}, \tag{13}$$

$$\mathrm{K}_{ei} = \frac{1}{C_{ei}} = \frac{\rho c^2}{V_i}, \tag{14}$$

$$L_{ei} = \frac{\rho(x_2-L_1)^2}{V_i}, \tag{15}$$

where i represents element number, C_{ei} is the compliance, and L_{ei} is the inductance of the element (Song, 2010).

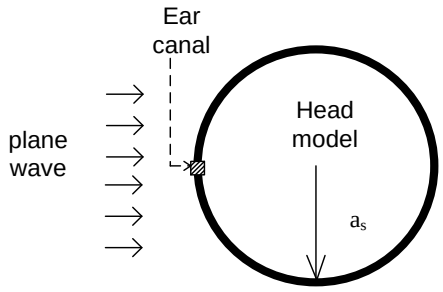

(a) Human head model

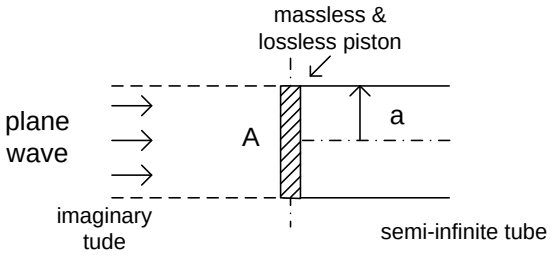

(b) Plane wave incident model in free-field

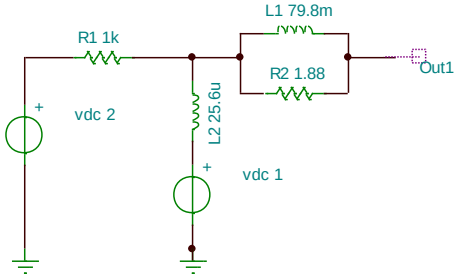

(c) Plane wave incident electric model

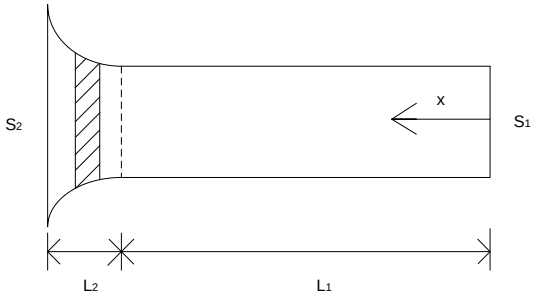

(d) Exponential model of external ear in AHAAH

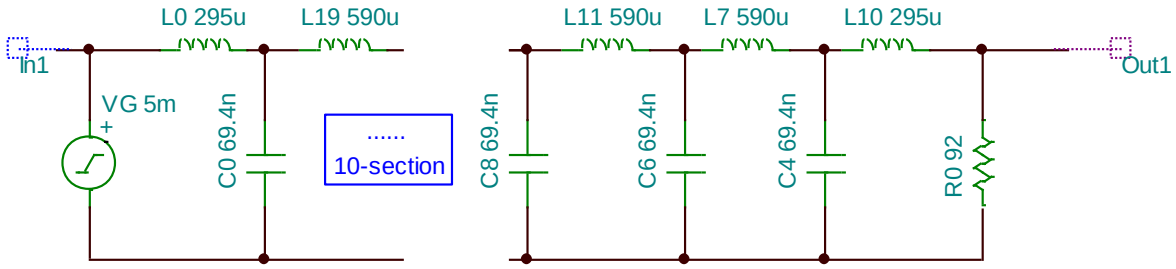

(e) Analog design of 10-section ear-canal analog network

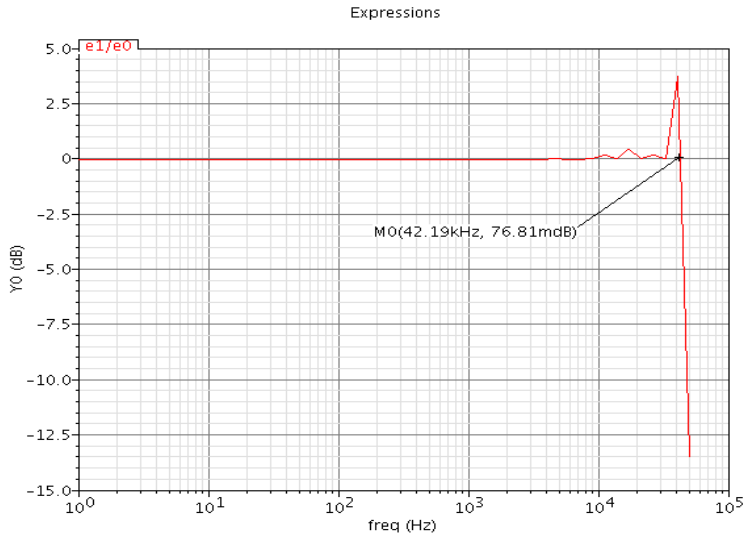

(f) Voltage-transfer characteristic for 10-section ear-canal analog network

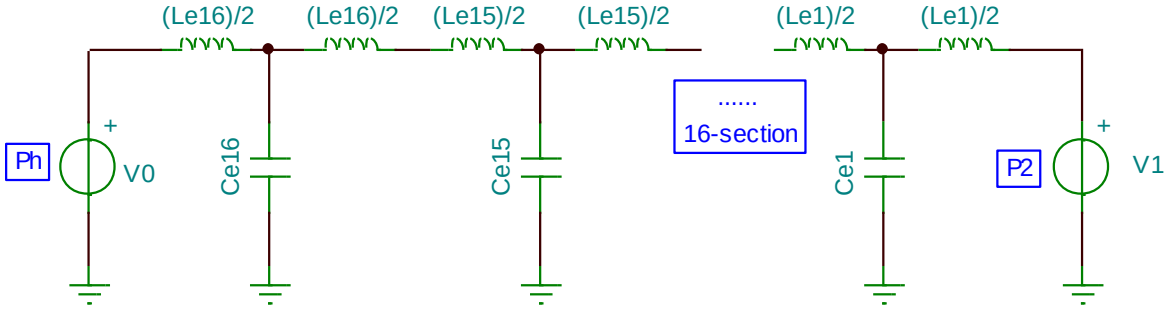

(g) Analog design of 16-section concha and ear-canal analog network in AHAAH model, where P_h is introduced from output of (c), and the P_2 is the input for the ear drum in middle ear

Figure 5 Human head model to simulate the external ear with a plane wave incident on a lossless and massless piston in the end of a long tube for free-field

2.2.2 Middle ear model of AHAAH

AHAAH uses the simple type of eardrum network topology to simulate the human middle ear model (Price, 2007). The middle ear elements in AHAAH model are designed based on the model first suggested by Zwislocki in 1962, and was revised by additional impedance elements given by Lynch in 1982 (Price, 1991).

Differences between AHAAH model and Zwislocki-model is the shunt impedance of malleo-incudal joint (M-I joint), and the incus Li is separated from the malleal complex block. The impedance networks in middle ear are realized as simple RLC circuits, while the effective area parameters are not clear from literatures (Song, 2010). Another time duration is added into middle ear part, called annular ligament segment, to simulate two options called ‘warned’ and ‘unwarned’ case in AHAAH model, different by the activation of the middle-ear acoustic reflex. It was designed as a time-delay component precedes the activation of the reflex to simulate the middle-ear protection mechanism (Price, 1991).

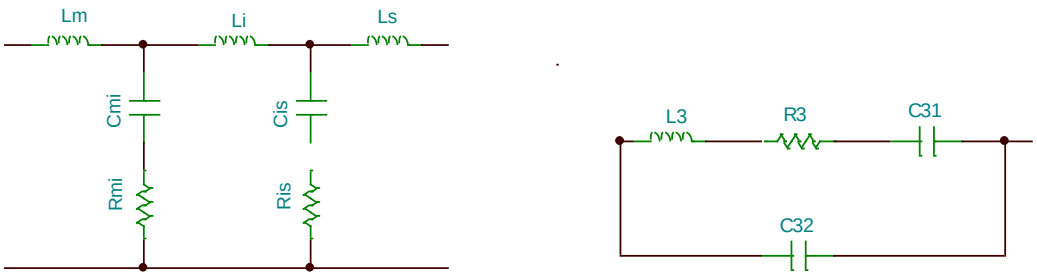

(a) Middle ear ossicular chain used in AHAAH model, network based on flexible M-I joint

(b) Network model of the human middle ear cavities in AHAAH model

Figure 6 Middle Ear network diagram

2.2.3 Inner ear model of AHAAH

In the cochlear modeling, the spiral shape of the cochlear bony wall is simplified into the two-channel fluid-structure system (shown in Figure 1) with input, the stapes vibrations, propagating a waveform inside cochlear segmentation. The transfer characteristic of cochlear model is a linear transfer function with ratio of the response output based on geometric

partitioned cochlea to the input. Hence, the displacement transfer function of the cochlea is as below,

$$H_D(x,\omega) = H_V(x,\omega) \times \frac{A_{fp}}{A_p(x)}, \tag{16}$$

$$H_v(x,\omega) = \frac{V_p(x,\omega)}{V_{ST}(\omega)}, \tag{17}$$

where A_{fp} represents the area of stapes footplate, A_p represents the area of cochlea partition area, and $V_p(x,\omega)$ and $V_{ST}(\omega)$ are volume displacements of the cochlear partition and the stapes respectively. In Zwislocki's model,

$$H_v(x,\omega) = H_0^{(2)}[\frac{2}{\beta}\sqrt{(\frac{\rho}{Q}\omega\frac{1}{jZ_P})}]\frac{Z_{CO}}{Z_P}, \tag{18}$$

$$Z_{CO} = [\frac{j4\pi\rho}{\sqrt{\alpha}\beta Q_0}]\frac{H_0^{(2)}(\sqrt{\alpha}f)}{H_1^{(2)}(\sqrt{\alpha}f)}, \tag{19}$$

where Z_P represents the cochlear partition impedance, Z_{CO}represents the cochlear input impedance evaluated at $x = 0$, ρ is the density of the cochlear fluid (/perilymph), Q is the effective sectional area of cochlear, Q_0 is the effective sectional area at the location $x = 0$ point of the stapes, $H_1^{(2)}$ is first order Hankel function of second kind, $H_0^{(2)}$ is the zero-th order Hankel function of second kind, α and β are defined angular coefficients to cochlea effective area partition respected to different frequency region (Song, 2010).

In AHAAH model, the method to calculate the displacements is to detect the velocity respectively from pressure and impedance, and to sum together each respectively located in 23 spaces along the basilar membrane about 1/3 octave intervals (Price, 2007). The related equation is as below,

$$ARU = sum(D^2), \tag{20}$$

where *D* denotes upward BM displacement (in microns), the magnitude of max BM max displacement (Price, 2007). AHAAH model does not provide full description for the impedance parameters, components of the cochlear impedance are represented per unit area in AHAAH model. In the magnitude of the cochlear partition impedance along the BM length from the base to the apex, two vertical lines represent the BM region of consideration in AHAAH.

Table 2 Parameter table for AHAAH model

Parameter Table	
Parameter	**Value**
Density of air (ρ)	1.15×10^{-3}
Speed of sound (c)	3.52×10^{-4}
Head diffraction field resistance (R_{df})	1.29×10^{-1} Ω
Head diffraction field inductance (L_{df})	2.56×10^{-5} H
Concha entrance radiation resistance (R_{pl})	1.88×10^{1} Ω
Concha entrance radiation inductance (L_{pl})	7.98×10^{-4} H
Radius of the piston (a)	5.0 cm
Radius of the head model (a_s)	9.99 cm
Concha entrance area	4.3 cm^2
Effective Area of piston for R_{pl}	2.15 cm^2
Effective Area of piston for L_{pl}	1.43 cm^2
Math model of canal L_1	2.215 cm
Math model of canal L_2	6.962×10^{-1} cm
Ear canal area connect to middle ear S_1	0.44 cm^2
Ear canal entrance S_2	4.3 cm^2
Eardrum conductive part, L_{dm}	22 mH
Incus, L_i	2440 mH
Bulla, C_m	4.33×10^{-4} μF
Malleo-incudal joint, R_{mi}	839100 Ω
Incudo-stapedial joint, C_{is}	4.57×10^{-4} μF
Incudo-stapedial joint, R_{is}	47500 Ω

Table 2 Parameter table for AHAAH model (Continued)

Parameter	**Value**
Stapes footplate area, A_{fp}	0.021 cm^2
Network model of the middle ear cavities, L_3	14 mH
Network model of the middle ear cavities, C_{31}	5.1μF
Network model of the middle ear cavities, C_{32}	0.35 μF
Network model of the middle ear cavities, R_3	91.85 Ω
$P_c/U_c=R_c$	6600 Ω
Cochlea, L_o	131 mH
Helicotrema, R_o	450 Ω
Stapes, L_S	6.1 mH
Vestibular volume, L_V	15.6 mH
Round window, C_{rw}	5.52 μF
Stapes footplate area (A_{fp})	2.1×10^{-2} (cm2)
Resistance of the cochlear partition (R_p)	$91.2\times e^{-x}$ (dyne-sec/ cm^3)
Compliance of the cochlear partition (C_p)	$1.0\times10^{-9}e^{1.50x}$ (cm^3/dyne)
Mass of the cochlear partition (M_p)	$5.8\times10^{-3}e^{-x}$ (g/ cm^2)
Width of the cochlear partition (w)	$0.8\times10^{-2}e^{0.5x}$ (cm)
Scala sectional area (Q)	$1.25\times10^{-2}e^{-0.5x}$ (cm^2)
Characteristic frequency (F_C)	$2.0\times10^{4}e^{-1.25x}$ (Hz)

CHAPTER 3

MATERIALS AND METHODS

3.1 Impulse noise generating system and measurement system

The noise-exposure system is designed to produce different kinds of noises in open field, such as Impulse noise and Gaussian noise (Johnston A. M., 2011), to simulate noise exposure in war field and industry environment. A microphone is used to acquire sound exposure data down from a shock tube, and send the data to ADC to be analyzed by computer software system. This study evaluates impulse noise by signal analysis method to measure hazardous factors in open field.

As shown in the Figure 7, the noise-exposure system consists of a control system based on LabVIEW software, a National Instruments (NI) data acquisition (DAQ) USB-6251, a Yamaha P2500S power amplifier, a JBL 2446H compression speaker (with an exponential horn) (Johnston M. A., 2011) and an signal analysis system developed by Matlab software. In the signal analysis system, we will bring discussions and results upon impulse noise by characteristic parameters both in time domain and frequency domain. Afterwards, collected impulse noises from the noise-exposure system will be extracted by feature parameters into following discussions, and be fed back to the AHAAH model to calculate the ARUs.

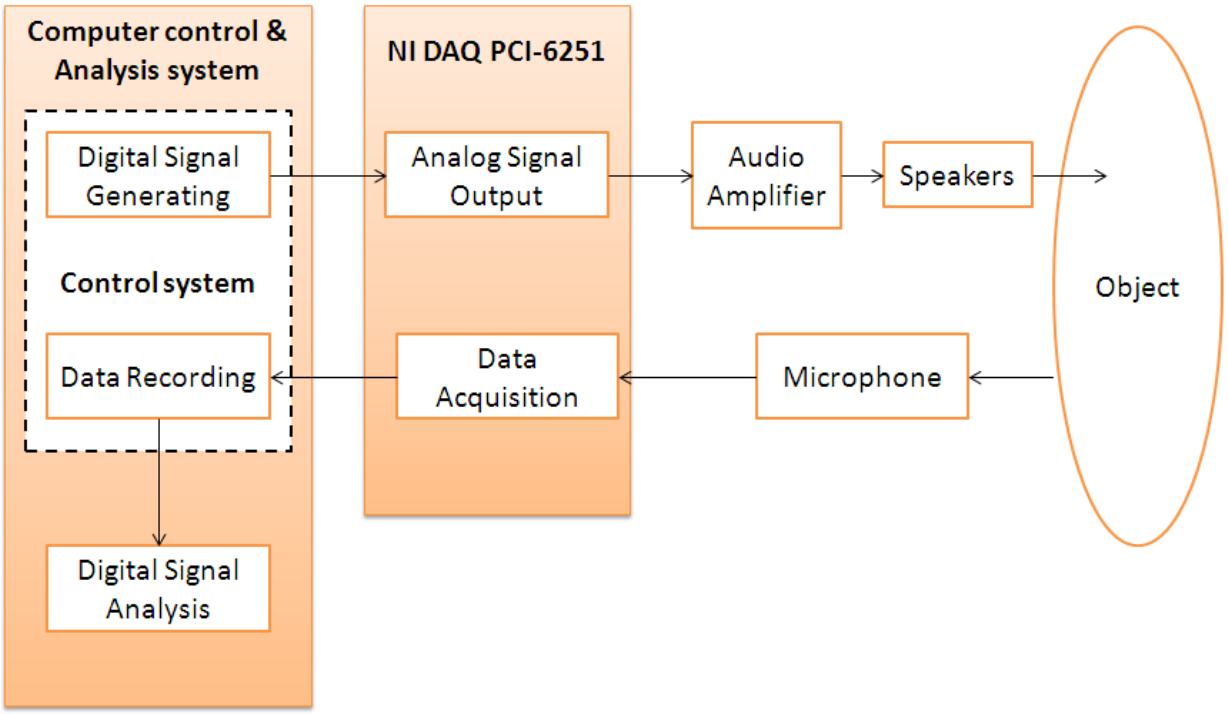

Data generated from this system aims to simulate the open field noise exposure. And this study mainly focuses on "Digital Signal Analysis" method realization by Matlab.

Figure 7 Schematic diagram of impulse noise exposure systemd

3.2 Experiments design

The digital impulse signals were generated and filtered by using LabVIEW software. Then, this program converts sound waves into analog impulse signals through one output channel of DAQ device. After amplification upon signal voltages, the analog impulse signals were sent back to the speaker to generate field-measured impulse noises. The generated impulse noises were measured and recorded by using a PCB 378C01 microphone (Johnston M. A., 2011). This microphone is combined with a preamplifier to output 20 voltage levels (i.e. 0.3 v, 0.5 v, 0.8 v, 1.0 v, 1.2 v, 1.5 v, 1.8 v, 2.0 v, 2.5 v, 3.0 v, 3.5 v, 4.0 v, 4.5 v, 5.0 v, 5.5 v, 6.0 v, 6.5 v, 7.0 v, 7.5 v, and 8.0 v). Ten waveforms were measured at each output voltage level. That is 200 data

measured in total. The outputs released afterwards are analyzed by statistic features or parameters, for example, the peak pressure versus voltage will be represented as the average peak pressure of 10 measured data at each voltage with standard deviation.

Experiments are designed first to simulate one cycle sine wave and evaluate effects of key parameters by AHAAH software, including amplitudes variances and time durations versus ARUs. Afterwards, we measured impulse noise from the noise-exposure system under different voltage drives, and loaded those data to get results in ARUs respectively for comparisons. In addition, we also use those measured data from the noise-exposure system to analysis amplitude, time durations, statistic kurtosis in time domain, 1/3-octave filter band frequency domain kurtosis (FDK) and FFT for frequency analysis.

3.3 Simulation of the sine wave for definition of key parameters

To evaluate the effect of each key parameter as shown in Table 1, firstly we simulated an impulse sequence by using the sinusoidal function in Matlab. Considering the discussion delivered in chapter 2.1.2 for the characteristic impulse noise, an impluse function can be simulated by sinusoidal sequence as definitions below,

$$\delta(t) = \lim_{T \to 0} p(t) = \begin{Bmatrix} \sin(t), & |t| \le T/2 \\ 0, & |t| > T/2 \end{Bmatrix}. \tag{21}$$

The integral of the sine signal impulse function is given by

$$\int_{-\infty}^{\infty} \delta(t)\, dt = -\cos(t)\,|_0^{T/2} = 1. \tag{22}$$

The sinusoidal impulse sequences were generated in Matlab (as shown in the Figure 8). Figure 8 (a) stands for one cycle sine wave form, which is cut into half cycle as “sine p-positive wave of half cycle” in Figure 8 (b) and “sine p-negative wave of half cycle” and in Figure 8 (c). By setting the values after the half sine cycles as “0”, the sequence for impulse noise is constructed shown in Figure 8 (d) and (e).

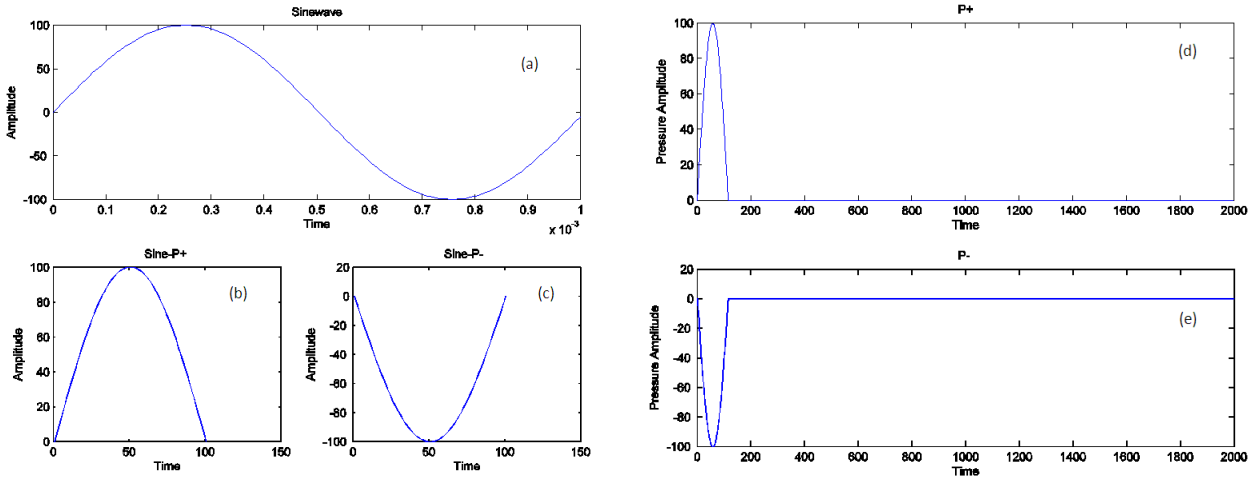

Figure 8 The generating process of sine impulse noise sequence using Matlab: (a) one cycle sine wave form, (b) positive half cycle sine wave, (c) negative half cycle sine wave, (d) sine positive pressure impulse sequence, and (e) sine negative pressure impulse sequence

The simulated sine impulse sequences were used to calculate the ARUs in the AHAAH model, and to investigate the effects of key parameters of impulse noise on auditory hazard.

3.4 Applications based on AHAAH model

In this thesis, we used an unmodified AHAAH model to investigate the effects of key parameters of an impulse noise. The software of AHAAH model (beta release W93e) was downloaded from the website of United States Army Research Laboratory, as shown in Figure 9.

All estimations of ARUs were calculated using “no protector, unwarned” setting in the AHAAH model.

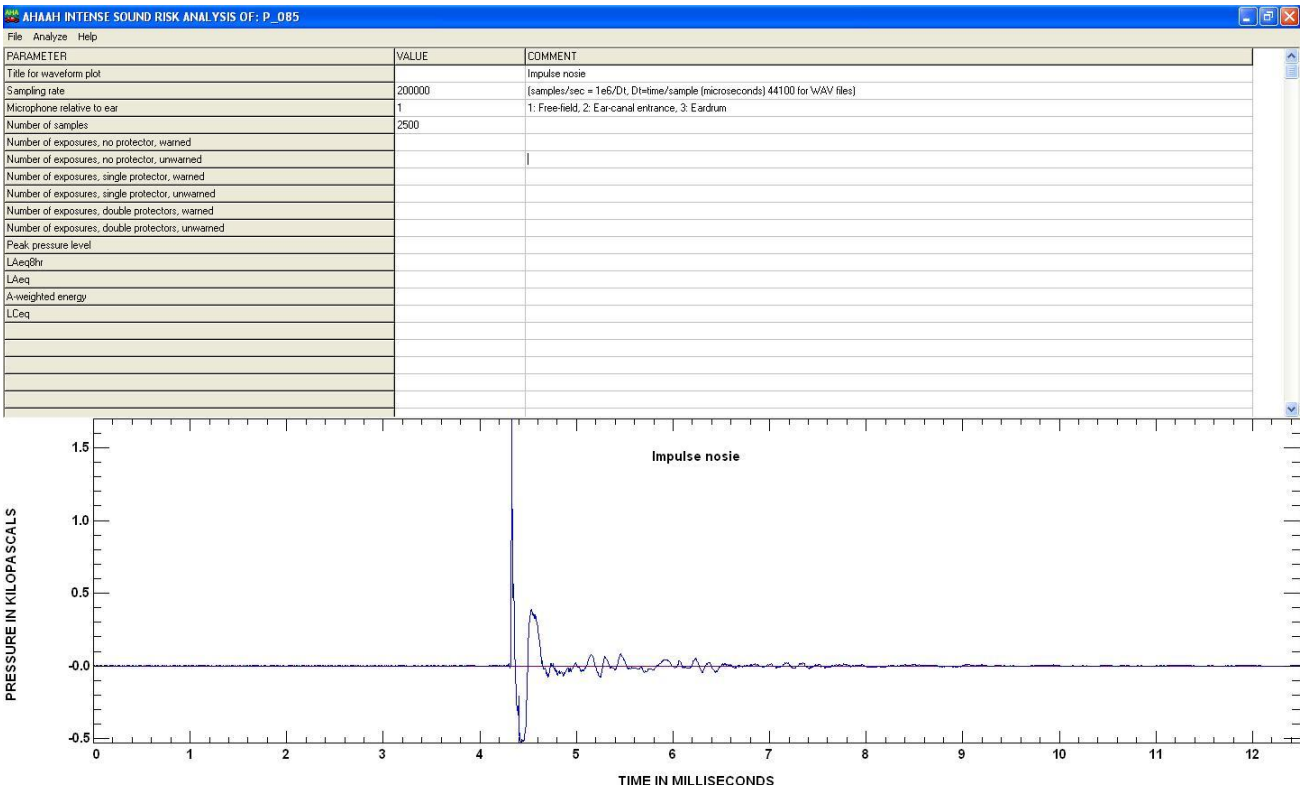

Figure 9 Interface of AHAAH software and related electrical circuit design

3.5 Frequency domain analysis

In this thesis, we also analyze the impulse noises by Fast Fourier Transform (FFT) and frequency domain kurtosis (FDK) in 1/3-octave filter bank.

3.5.1 FFT

Discrete Fourier transform (DFT) relates to Fourier Transform via the FFT sampling issues suggested under Nyquist criterion, and zero padding in the frequency domain as resolution. It also neglects the negative frequency components. In this thesis, we use matlab

function “fft” to realize the FFT frequency analysis upon impulse noises based on Cookely-Tukey FFT algorithm from matlab FFTW library. Given vector x[n], related equation as below,

$$X[k] = \sum_{n_2}^{N_2-1} \sum_{n_1}^{N_1-1} x[n_1 N_2 + n_2] W_{N_1}^{n_1 k_1} W_{N_2}^{n_2 k_2} \quad (23)$$

where $n = n_1 N_2 + n_2$, $k = k_2 N_1 + k_1$ ($n_1 \in [0, N_1 - 1], n_2 \in [0, N_2 - 1], k_1 \in [0, N_1 - 1, k2 \in 0, N2 - 1$).

To demonstrate the FFT of acoustic signal in power spectra density (PSD), we use definition as below (Dwyer, 1984). We also use dB unit for PSD (i.e. P_dB(X)) for the final results demonstration.

$$P(X) = (\frac{1}{n}) \sum_{q=1}^{n} X[k] X^*[k], \quad (24)$$

$$P\_dB(X) = 10 \times log_{10} P(X). \quad (25)$$

3.5.2 Frequency domain kurtosis (FDK)

To use statistic kurtosis in the frequency domain is to compare the PSD by characteristic kurtosis computed as a technique of signal analysis in frequency domain (Dewey, 2004). We already talked about the definition of kurtosis in previous chapter based on its physical and mathematical definition (i.e. the expected value of the fourth-order central moment ratios to the squared of the expected value of the second-order central moment separately). Impulse noise is assumed as a zero-mean process input, and the acoustic propagation is considered as a fading received data including the phase fluctuations into an independent zero-mean stationary process (Dewey, 2004) (Erdreich, April 1986). For example, impulse noise measurement by the noise-exposure system in one cycle (under sampling frequency 65536 Hz), 1800 Pa peak pressure

measured in A-duration (0.2 ms) versus 0 Pa peak pressure measured in the rest time (999.8 ms), the average of the signal is almost zero. Hence, FDK calculated in acoustic field offers another perspective in statistic metrics to indicate the relationship between magnitude and frequency distribution of the acoustic trauma (Roberto, Hamernik, Salvi, Henderson, & Milone, 1984) .

Based the definition of FDK, it uses DFT to convert waveforms from time domain to frequency domain, and estimate the power spectrum densities. The FDK estimates the real part for sequence *x(i, q)* after DFT by distinct frequency components (where *i* and *q* together represent the real discrete data) as below,

$$x(i,q) = x[(i + (q-1)M)h], (i = 0, 1, \dots, M-1;\ q = 1, 2, \dots, n), \tag{26}$$

$$K(F_p) = \left(\frac{1}{n}\right) \sum_{q=1}^{n} \left(X(q, F_p)\right)^4 / \{(\frac{1}{n}) \sum_{q=1}^{n} (X(q, F_p))^2\}^2 , \tag{27}$$

$$f_p = \frac{p}{Mh}\ Hz , \tag{28}$$

where F_p represents the p_{th} radian frequency component, *h* is the interval between successive observations of the process, *p* = 0, 1, … , *M-1*, and we also simplified the *h* = 1 in the future computational convenience (Dwyer, 1984).

According to the ANSI S1.11 Standard, 1/3-octave bands covering the frequency range from 0 Hz to 20 KHz (D. Tharini, 2012). In order to simulate the 1/3-octave intervals partition in cochlea, we introduce a band-pass filter with bandwidth defined in 1/3-octave filter bank ranged from 0 Hz to 20 KHz. To extract the related components within the cut-off frequencies, we first filtered the signal in time domain and then use FFT to transfer it to frequency domain. By using these frequency components, we calculate the kurtosis as defined previously for FDK in each

1/3-octave interval. Each 1/3-octave bank is defined by one central frequency f_0, and the bandwidth B. f_0 of the nth band with bandwidth B, and related cut-off frequency f_1 and f_2 are followed as equations below,

$$f_0(n) = 2^{n-30/3} \times f_r, \tag{29}$$

$$f_1(n) = f_0(n) \times 2^{-1/6}, \tag{30}$$

$$f_2(n) = f_0(n) \times 2^{1/6}, \tag{31}$$

$$B(n) = f_2(n) - f_1(n), \tag{32}$$

where f_r is the reference frequency valued 1 KHz. We use Butterworth band-pass filter to realize the FIR filter function as shown in Figure 10 (a). The 1/3 octave filter band is designed with central frequency f_0 range from 0 Hz to 20 KHz. In FDK calculation, we still keep using the segmentation idea of M in statistic kurtosis of time domain, in order to evaluate the effective metric of FDK for acoustic hazard purpose with affect by zero padding. In FDK calculation shown in results part, we set M = 1.9 ms.

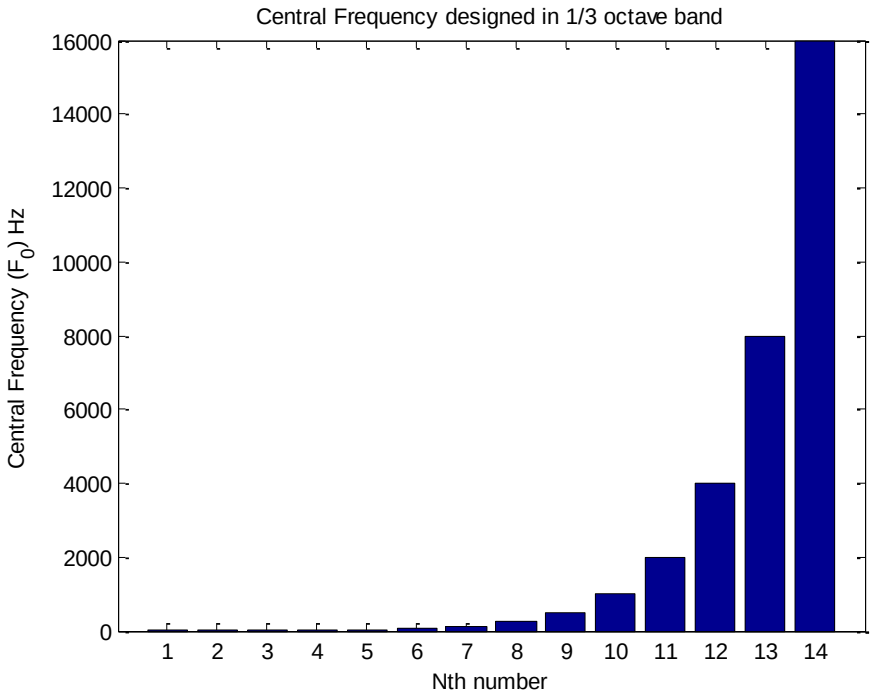

(a) Central Frequency in 1/3 octave band

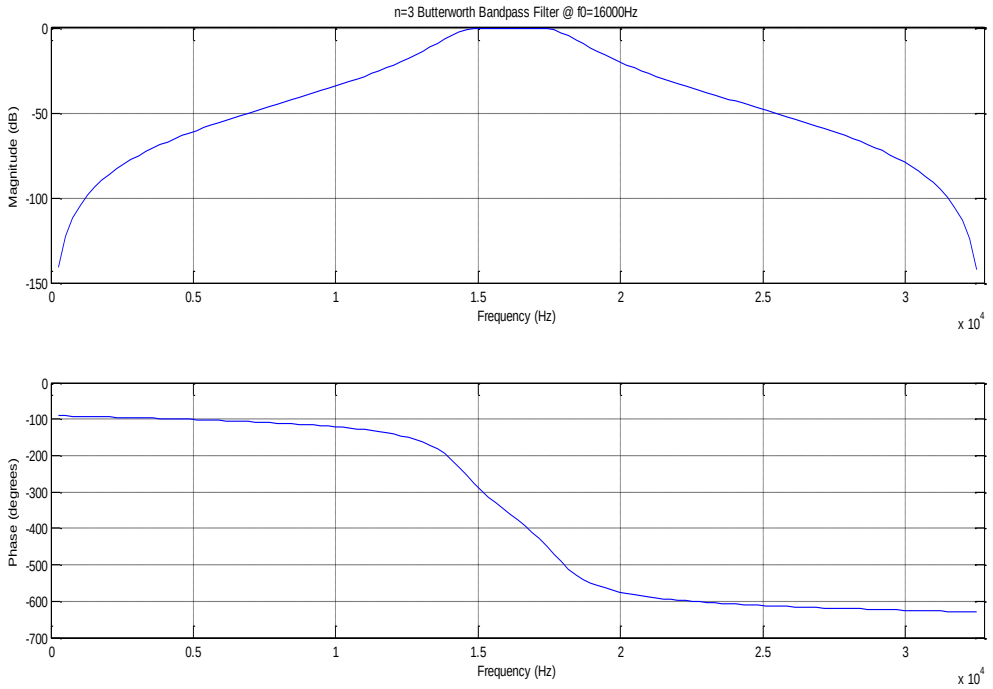

(b) 3rd order filter of Butterworth band-pass filter @ central frequency 16 KHz

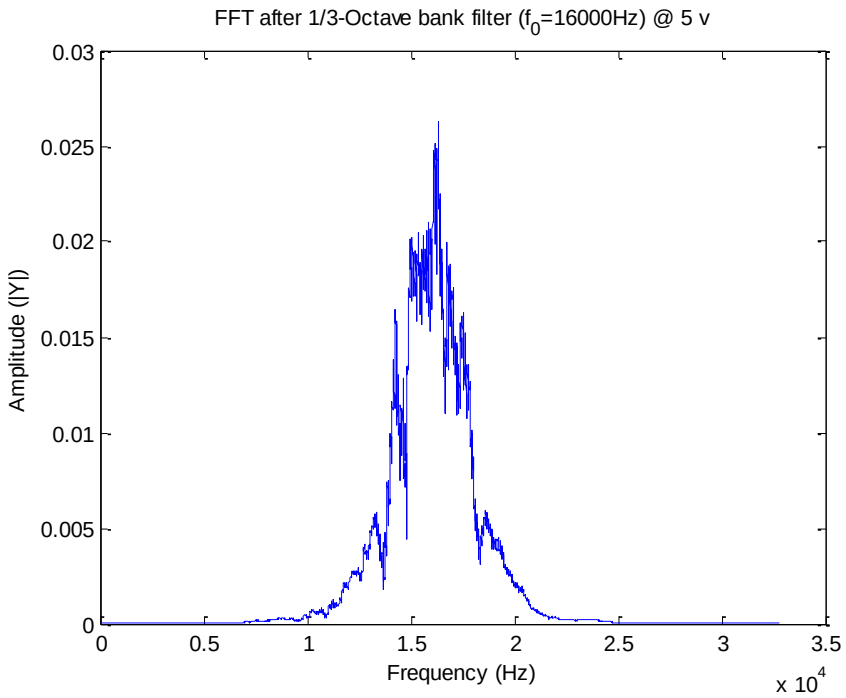

(c) FFT after 3rd order filter of Butterworth band-pass filter @ central frequency 16 KHz

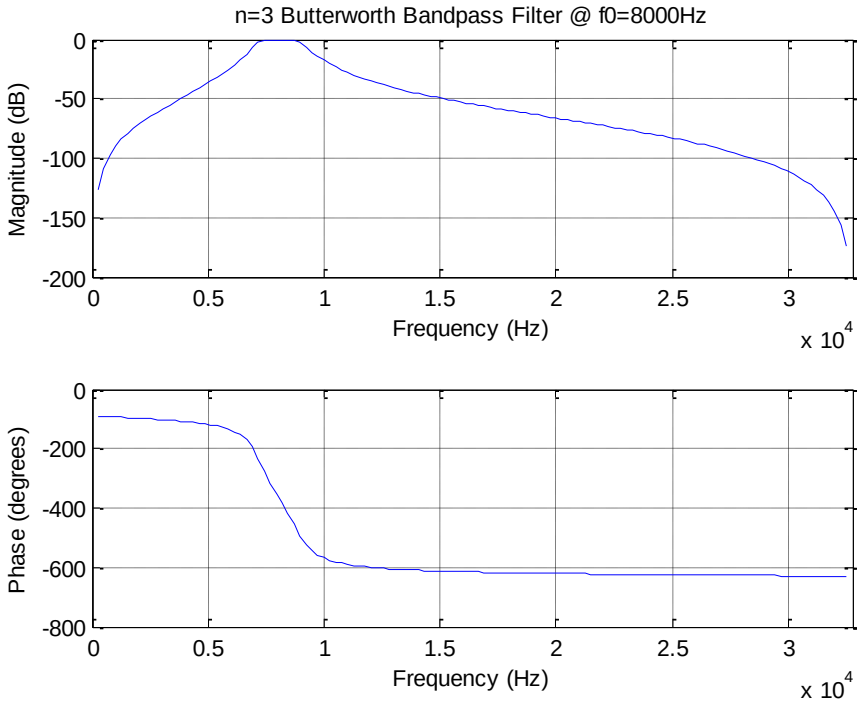

(d) 3rd order filter of Butterworth band-pass filter @ central frequency 8 KHz

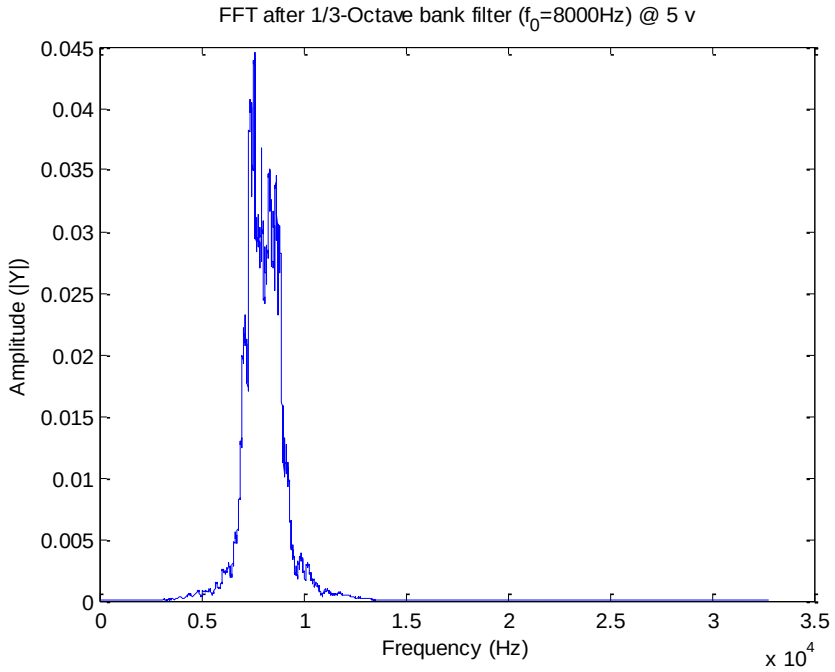

(e) FFT after 3rd order filter of Butterworth band-pass filter @ central frequency 8 KHz

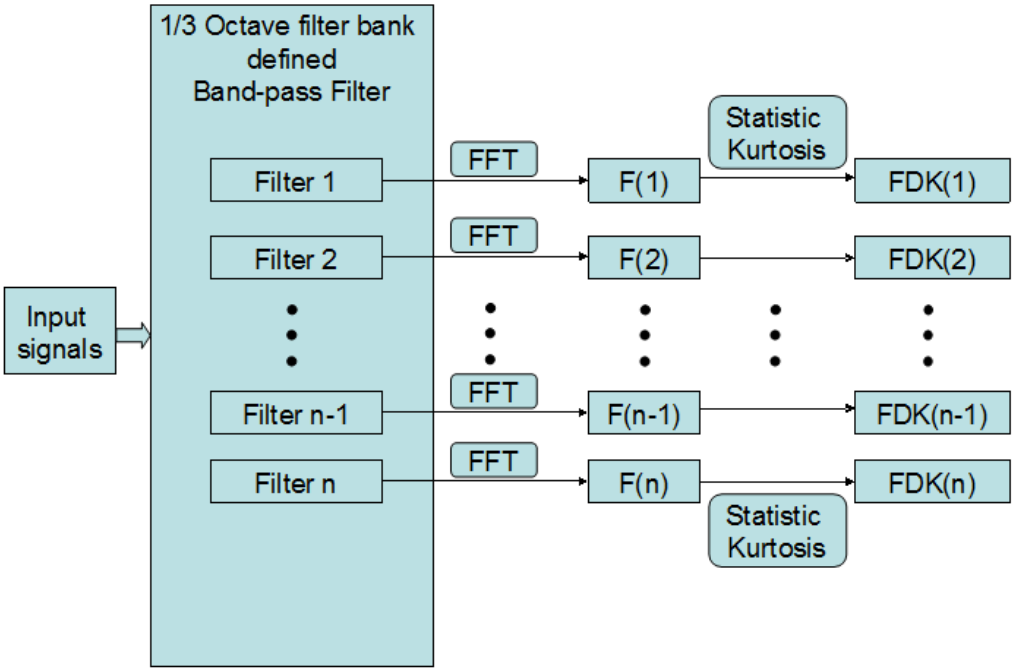

(f) FDK realization by 1/3 Octave bank filter

Figure 10 FDK design process

CHAPTER 4

RESULTS: CHARACTERISTIC OF IMPULSE NOISE

4.1 Time domain analysis results

A typical acoustic impulse noise, which is generated from the noise-exposure system at voltage 5 v, is shown in Figure 11 as below. It illustrates that the impulse noise has an envelope which is firstly led by a compressive pulse at the peak pressure of about 158.4 dB SPL, then followed by a negative peak pressure, and is ended in oscillation tails, with a comparable time duration to a measured field impulse noise. This typical acoustic impulse noise is used to simulate impact noise leading to hearing injuries in military standard, especially being replicated and tested in M-16 rifle research (Price, 2010).

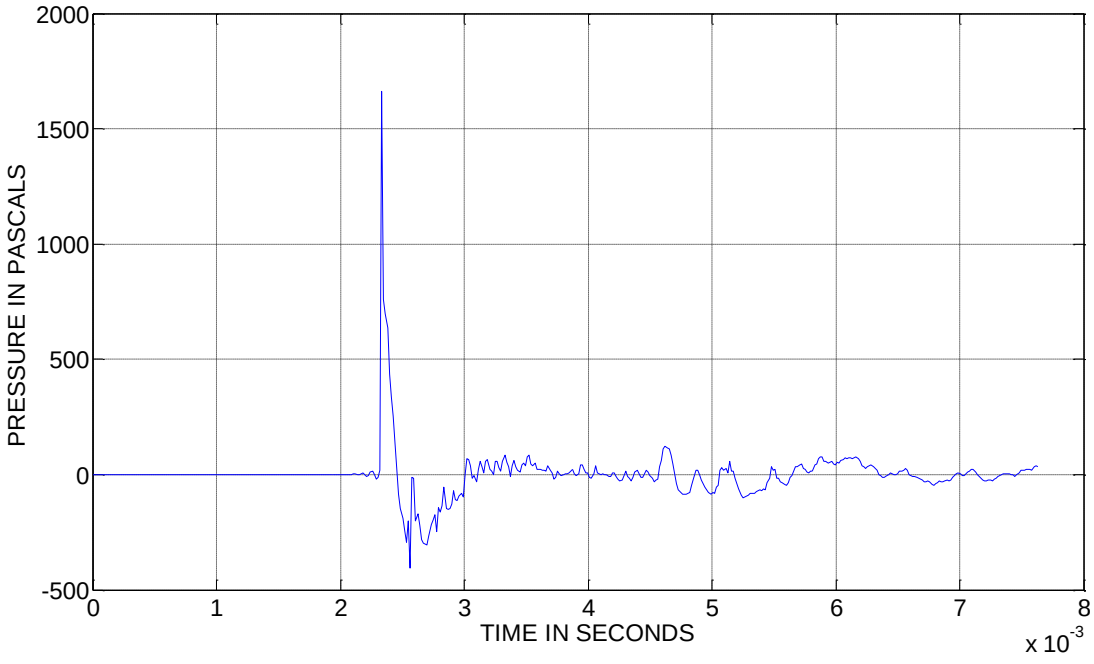

Figure 11 Impulse noise waveform generated from the noise-exposure system

4.1.1 Amplitude

Figure 12 illustrates the average peak pressures at various voltages and the corresponding standard deviations. These statistics are calculated by 10 independent tests at each voltage. From Fig.12, on can see the average peak presure is monotonically increasing as the voltage is increasing, and later is approaching to a saturation. A polynominal curveis used to fit these measurements.

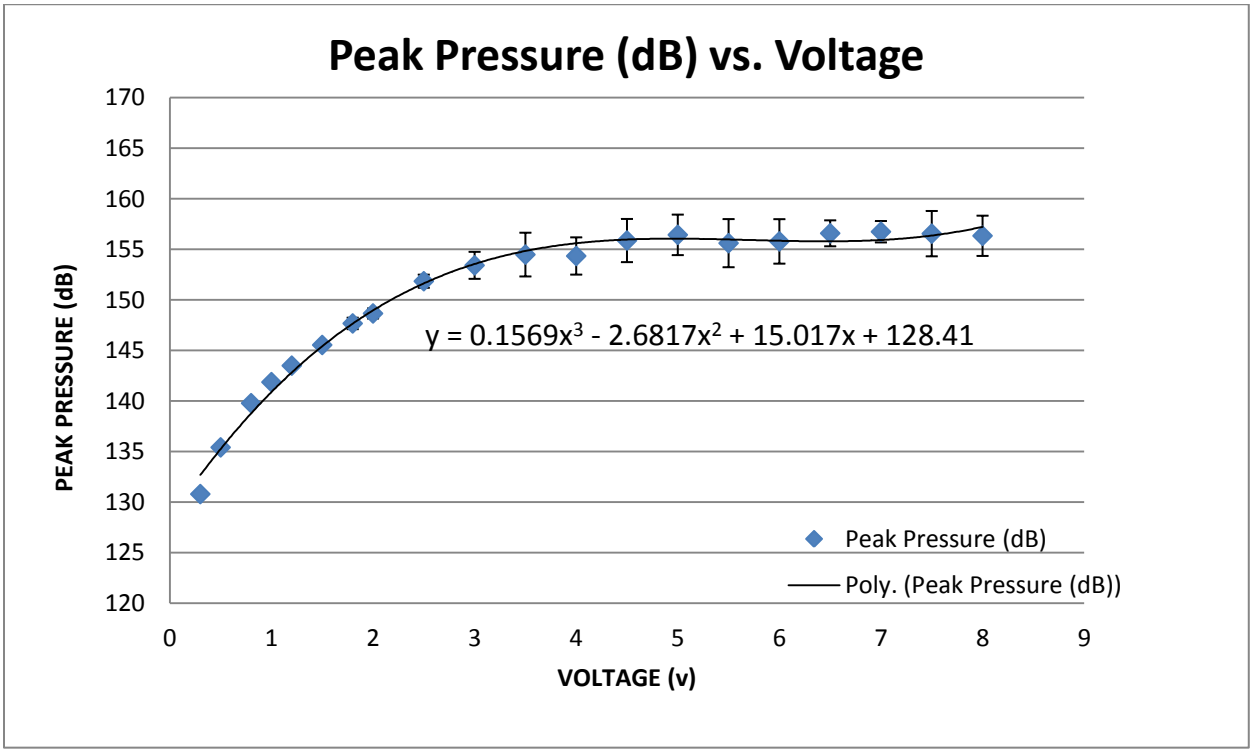

Result shows a monotonically increasing curve (Test data were measured ten times at each voltage generated by the system). And a saturation exists in higher voltages.

Figure 12 Peak pressure (dB) vs. voltage (v) of the noise-exposure system

4.1.2 A-duration time (t^+) & negative time duration (t^-)

Figure 13 illustrates A-duration time (t^+) and negative time duration (t^-) versus voltage by using measured impulse noises from the noise-exposure system (i.e. 10 signals are measured at each voltage, for 20 voltages , there are 200 signals in all). Basically, both A-duration time (t^+) and negative time duration (t^-) , first decrease before a particular voltage, and then tend to increase, in the form of a cycle-like tendency as shown below. In addition, negative time duration is longer than A duration.

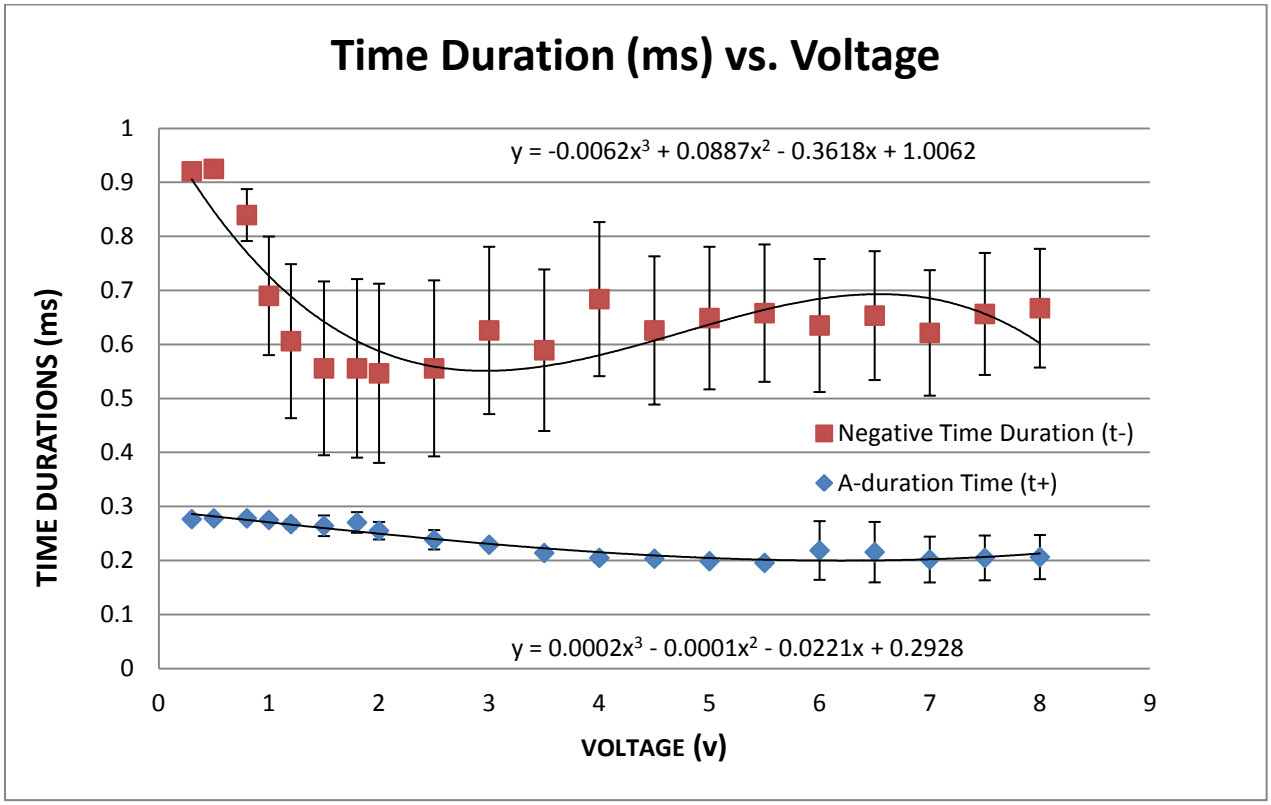

Both the two curves above show a cycle-like tendency of time durations withvoltage increasing. Negative time duration is longer than A duration

Figure 13 Time durations (ms) vs. voltage (v) of the noise-exposure system

4.1.3 Statistic kurtosis in time domain

Figure 14 shows the relationship between voltage increasing and statistic kurtosis of impulse noise in time domain, where random variables are selected in sampling space of a time cycle M = 1.2 ms in order to cover both peak and entire waveform of the impulse noise. A fitting curve of increasing distribution trends in Figure 14 demonstrates the amplitude-related statistic kurtosis versus to voltage increasing. Since 2.98 stands for kurtosis of Gaussian noise generated by the noise-exposure system, result shows that non-Gaussian components are increasing with voltage increasing in time domain.

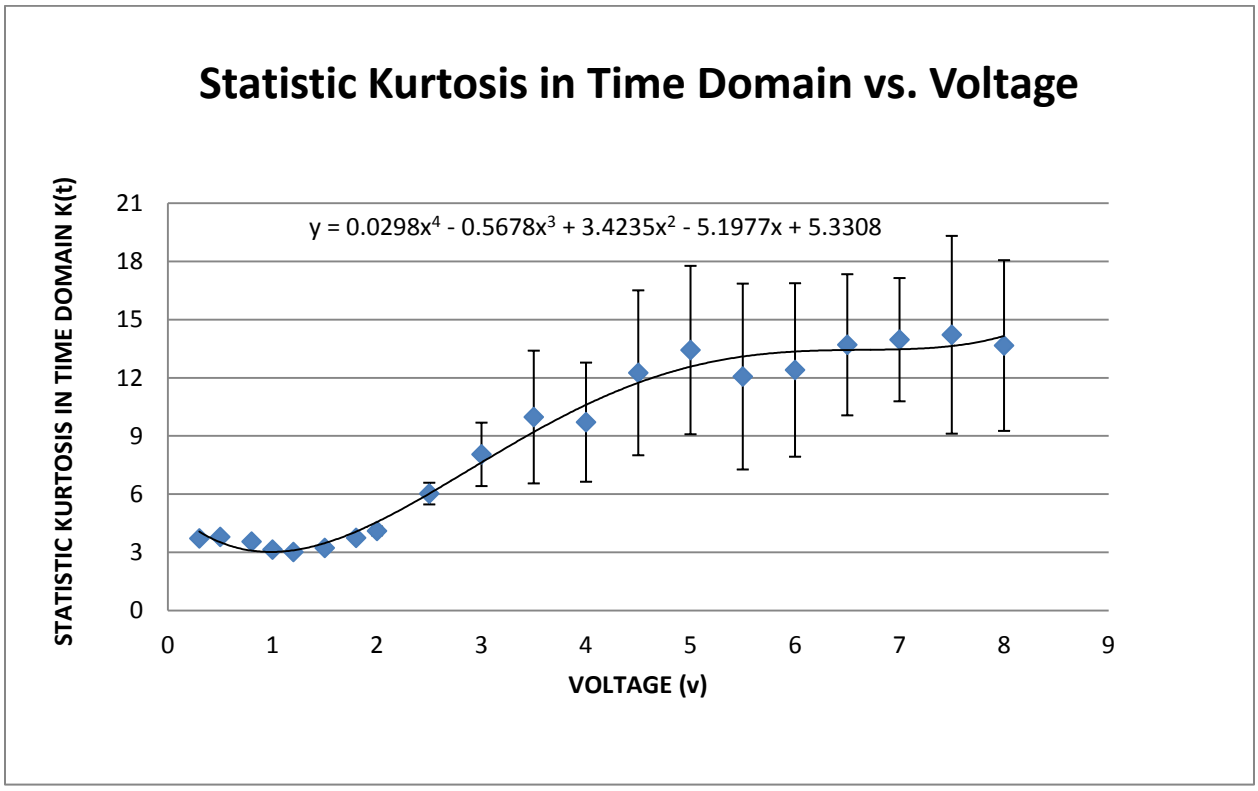

According to 2.98 kurtosis of Gaussian noise generated by the noise-exposure system, result shows that non-Gaussian components increase with voltage increasing in time domain (use time segmentation of M = 1.2 ms to include the peak and entire wave of impulse noise).

Figure 14 Statistic kurtosis vs. voltage (v) in time domain

4.1.4 L_{Aeq} & L_{Aeq_8h}

Figure 15 shows that the output energy of impulse noise increases with the voltage increase by the noise-exposure system, and saturates in higher voltages. Two polynomial curves present that L_{Aeq_8h}, which is estimated under each voltage, equals to L_{Aeq} decreased by an negative constant "-44.5939 (i.e. $10\times\log_{10}(1/28800)$) ". This is because that the continuous exposure condition of 8 hours (i.e. 28800 seconds) is introduced to bring down the noise energy. Hence, the continuous exposure time has an non-ignored effect in acoustic energy measurement, since the equivalent energy output of a typical impulse noise is proportional increased with exposure time increasing.

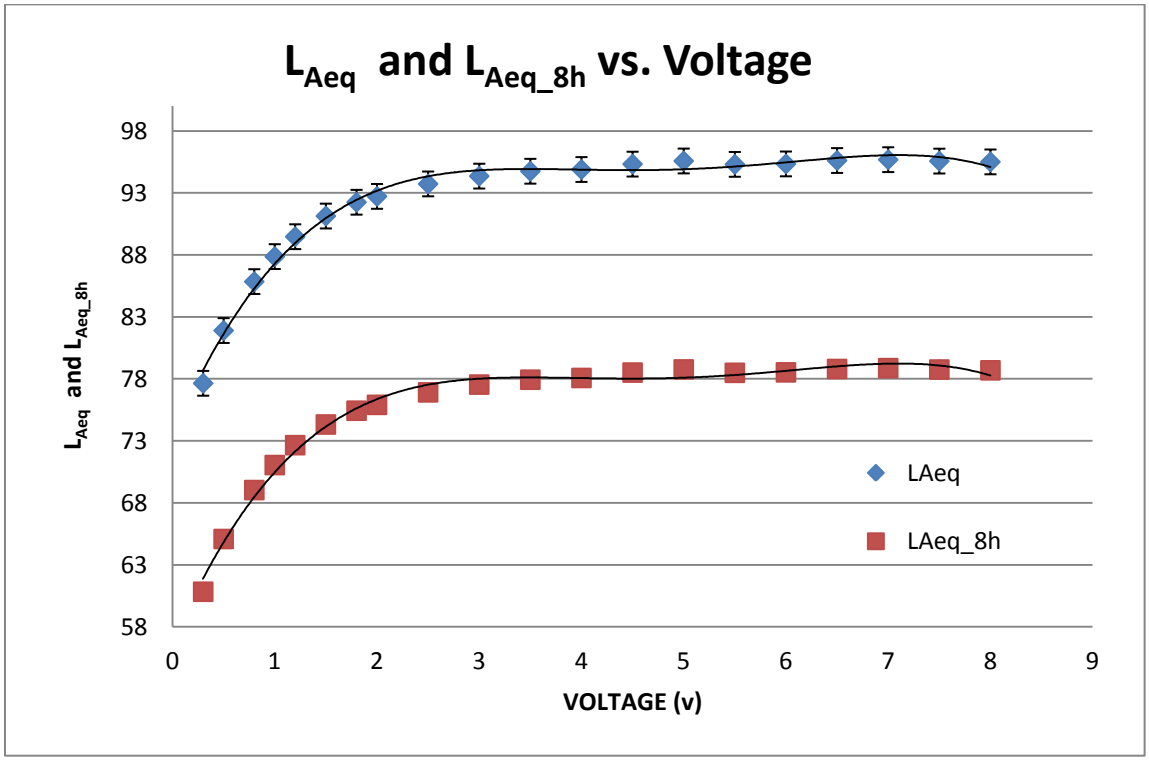

Two polynomial curves represent the L_{Aeq} is decreased by an negative constant "-44.5939 (i.e. $10\times\log_{10}(1/28800)$" to reach L_{Aeq_8h} introduced by the continuous exposure condition of 8 hours (i.e. 28800 seconds) under each voltage (where t_2-t_1=T=1 s).

Figure 15 Energy vs. voltage

4.2 Frequency domain analysis

4.2.1 FFT

Shown as in Figure 16, the FFT transform results display power spectra density (PSD) in Y-axis. By analyze the impulse noises at six different voltages generated from the noise-exposure system, the amplitudes in Y-axis increase with frequency increasing in X-axis. PSD of high frequency components increases with voltage increasing.

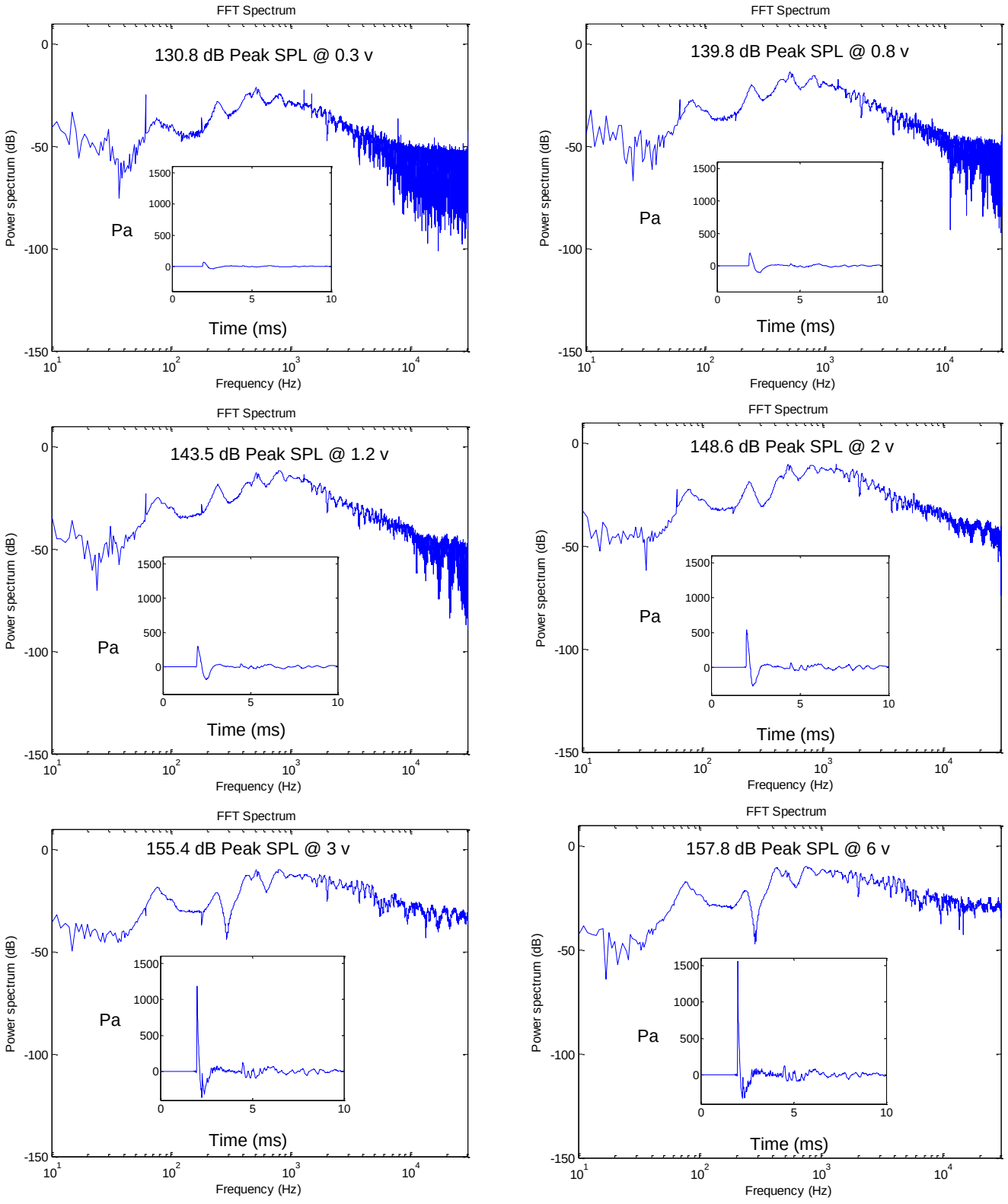

Figure 16 FFT plots of impulse noises

4.2.2 Frequency domain kurtosis (FDK)

By using 1/3-octave filter bank, which was implemented by a band-pass filter, frequency components firstly were filtered into bandwith of 1/3-octave band, after FFT, and were computed into statistic kurotsis in frequency domain. Consider the statistic characteristics of FDK, zero padding or more related similar frequencies components can affect FDK results. We introduce M segmentation as previously defined in time kurtosis to avoid zero padding affect.

In FDK, *M* is set as 1.9 ms before FFT, in order not only to cover the peak and entire waveform of impulse noise, but also to ignore the zero padding affection to statistic kurtosis calculation. FDK results in different voltages are as shown in Figure 17. Among 1.2 v, 3 v, 7 v, results demonstrate a similar fitting curve distribution, which presents the uniformed impulse noise distributed in frequency domain by the noise-exposure system.

Results are using “f2” (i.e. the max frequency of each 1-3 octave filter bank) for demonstration. Max FDK represents the max non-Gaussian components existing. Results show that turning points are before 140 Hz and 2245 Hz, FDK first increases with frequency increasing till peak, and then decreases with frequency increasing afterwards.

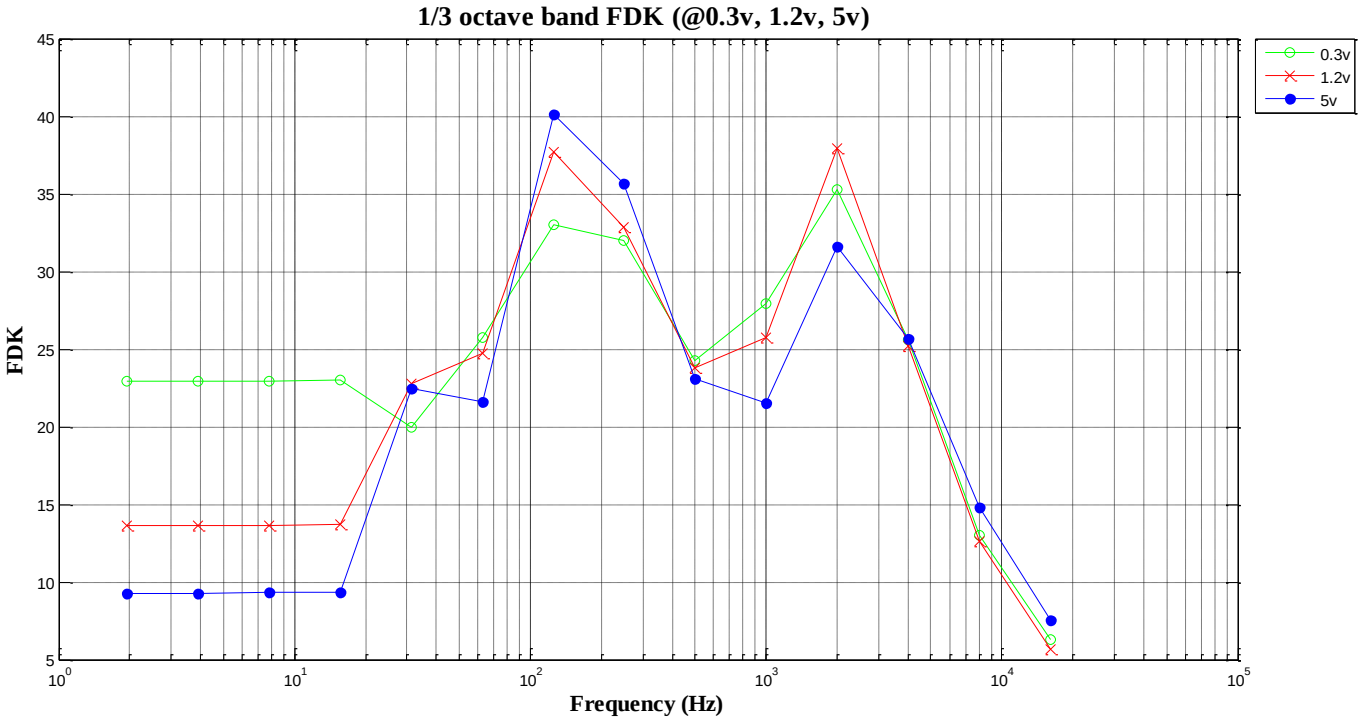

Figure 17 The profiles show the comparisons with the frequencies domain kurtosis (FDK) of impulse noises generated by different voltages in the noise-exposure system

CHAPTER 5

KEY PARAMETER EFFECT IN AHAAH

In this chapter, ARUs are firstly evaluated by simulated sine impulse sequences, and then by measured data from the noise-exposure generator. AHAAH model software is used to compare the characteristic impulse noise with predicted noise hazardous level in ARUs.

ARU of a sine p^+ impulse sequence

Figure 18 shows the ARU generated by a sine p-positive impulse sequence with peak pressure P = 2.5 KPa and time duration t = 0.2 ms. In Figure 18 (b), the stapes displacement shows a less active envelope than the waveform of sine p-positive impulse sequence (shown in the Figure 18 (a)). It reveals the organ protection from outer ear and middle ear (Guinan & Peake, 1967) (Price, 1965). BM displacement in Figure 18 (c) shows less activity at the apex of cochlea, however, the hazard function shows that its peak appears in mid-cochlea (Price & Kalb, 1991).

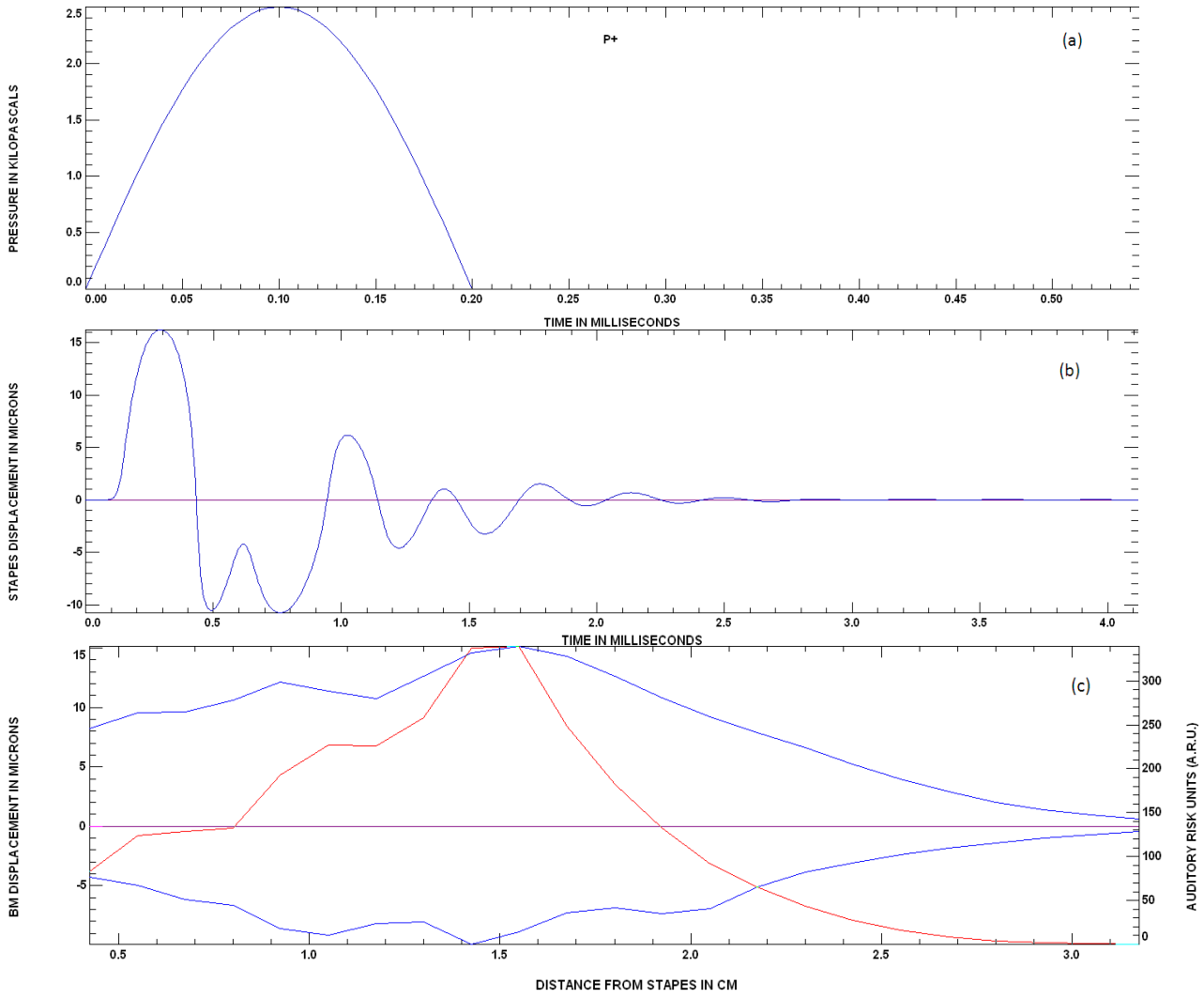

Figure 18 The ARU evaluation of a representative sine p-positive impulse sequence at P = 3.5 KPa and t = 0.2 ms. (a) Pressure waveform of p-positive impulse sequence, (b) the displacement of stapes in human ears yielded by P^+, and (c) the BM displacement and ARU change at different distance from the stapes in human ears

ARU of a sine p^- impulse sequence

Figure 19 illustrates that the ARU generated by a sine p-negative impulse sequence with peak pressure P = 3 KPa and time duration t = 0.2 ms. Compared to Figure 18 (b), Figure 19 (b) presents an inverse envelop on stapes displacement, which means the stapes move to an opposite

direction. Figure 19 c shows BM vibration reaches peak in mid-cochlea, which is consistent with the observation in Figure 18 (c).

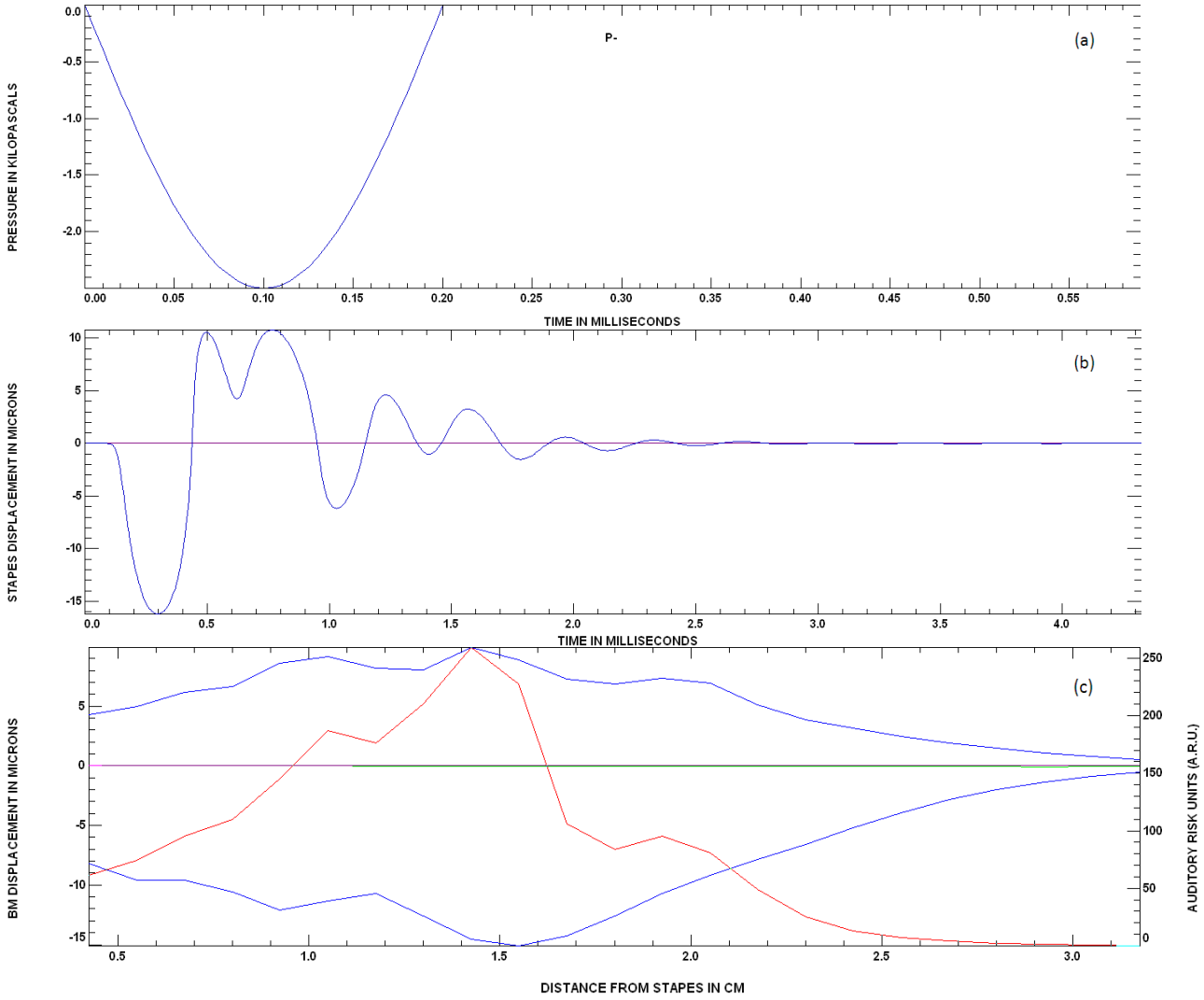

Figure 19 The ARU evaluation of a representative sine p-negative impulse sequence at P=-3 KPa and t=0.2 ms. (a) pressure waveform of p-negative impulse sequence, (b) the displacement of stapes in human ears yielded by P^-, and (c) the BM displacement and ARU change at different distance from the stapes in human ears

Peak pressure vs. ARU

Combine both sine p-positive impulse sequences and sine p-negative impulse sequences with variable peak pressures and unique time duration (t = 0.065 ms), Figure 20 shows the

relationship between the ARUs and the peak pressures in AHAAH model. The ARUs increase with both peak positive pressure (P^+) and peak negative pressure (P^-) increasing. However, the P^+ generates higher ARU than the P^- when the peak absolute pressure greater than 4 KPa. It may indicate that P^+ could be more hazardous than P^- at high pressure level. In addition, there is no significant difference of ARUs generated by P^+ and P^- at lower pressure level ($|P|< 4$ KPa).

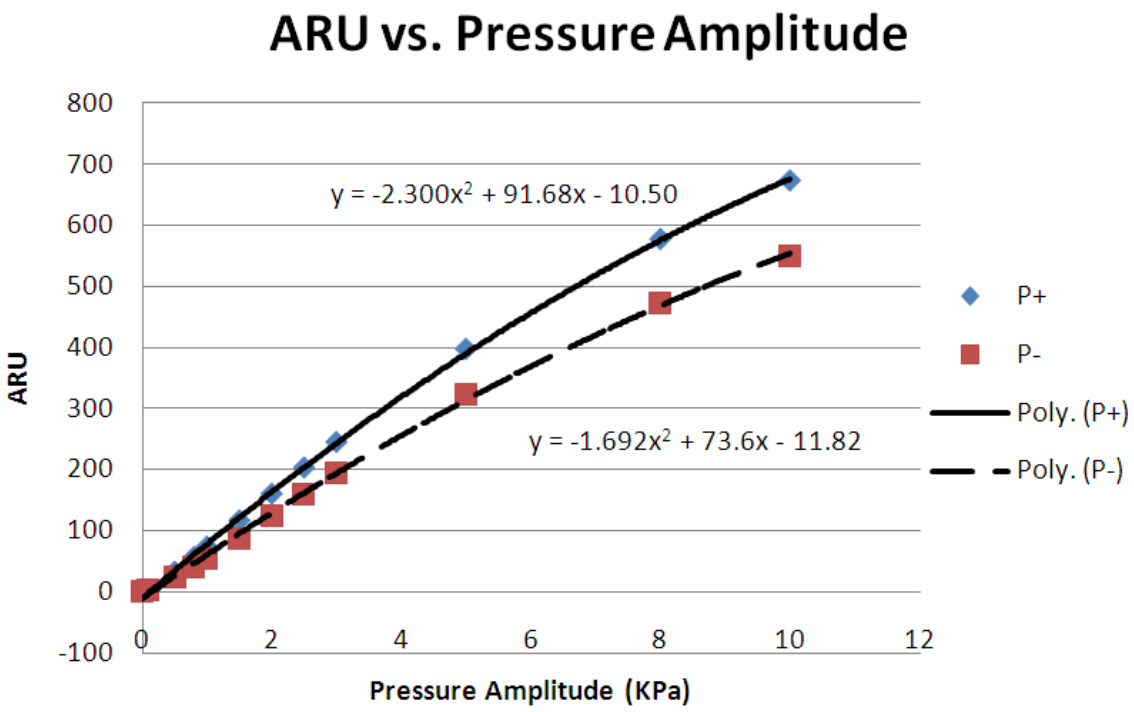

Figure 20 Relationship between ARUs and peak pressure (P^+ and P^-) with t = 0.065 ms

Time duration vs. ARU

Combine both sine p-positive impulse sequences and sine p-negative impulse sequences with variable time durations and unique peak pressure (P = 1 KPa), Figure 21 demonstrates the effects of the time duration on ARUs in AHAAH model. With both t^+ and t^- increasing, ARU increases when t < 0.2 ms, and then it decreases when t > 0.2 ms. However, the time duration of a field measured impulse noise (i.e. rifle impulse) is typically short, the hazard calculation grows

only in the first few milliseconds (Price & Kalb, 1991). In addition, the ARUs generated by the p-positive impulse sequences are greater than those by the p-negative impulse sequences. Compared to

Figure 13, t^- is a longer time duration compared to t^+, which is also the time-duration feature of the impulse noise. These results indicate that the t^+ affect more on the ARU estimation in the AHAAH model than the t^-.

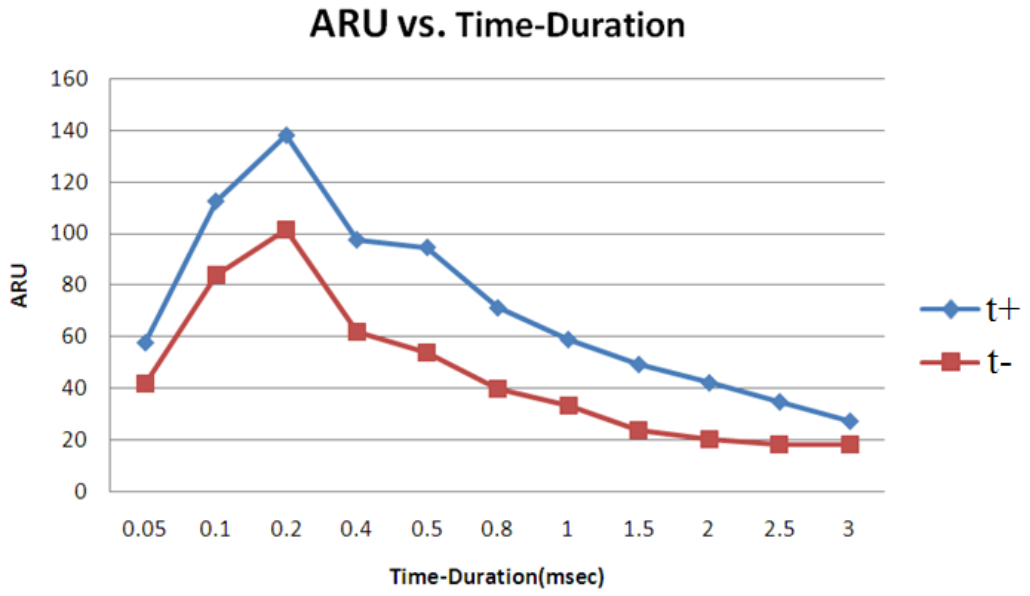

Figure 21 Relationship between ARUs and time duration (t^+ and t^-) with P = 1 KPa

ARU of a typical measured impulse wave by the noise-generator system

Figure 22 demonstrates estimation of ARU in AHAAH produced by a measured impulse noise waveform (with peak sound pressure level (SPL) = 155 dB) from the noise-exposure system. Some clippings can be seen in the stapes displacement in Figure 22 (b). One can observe that impulse noise causes stapes displacement with the same direction as the impulse noise waveform.

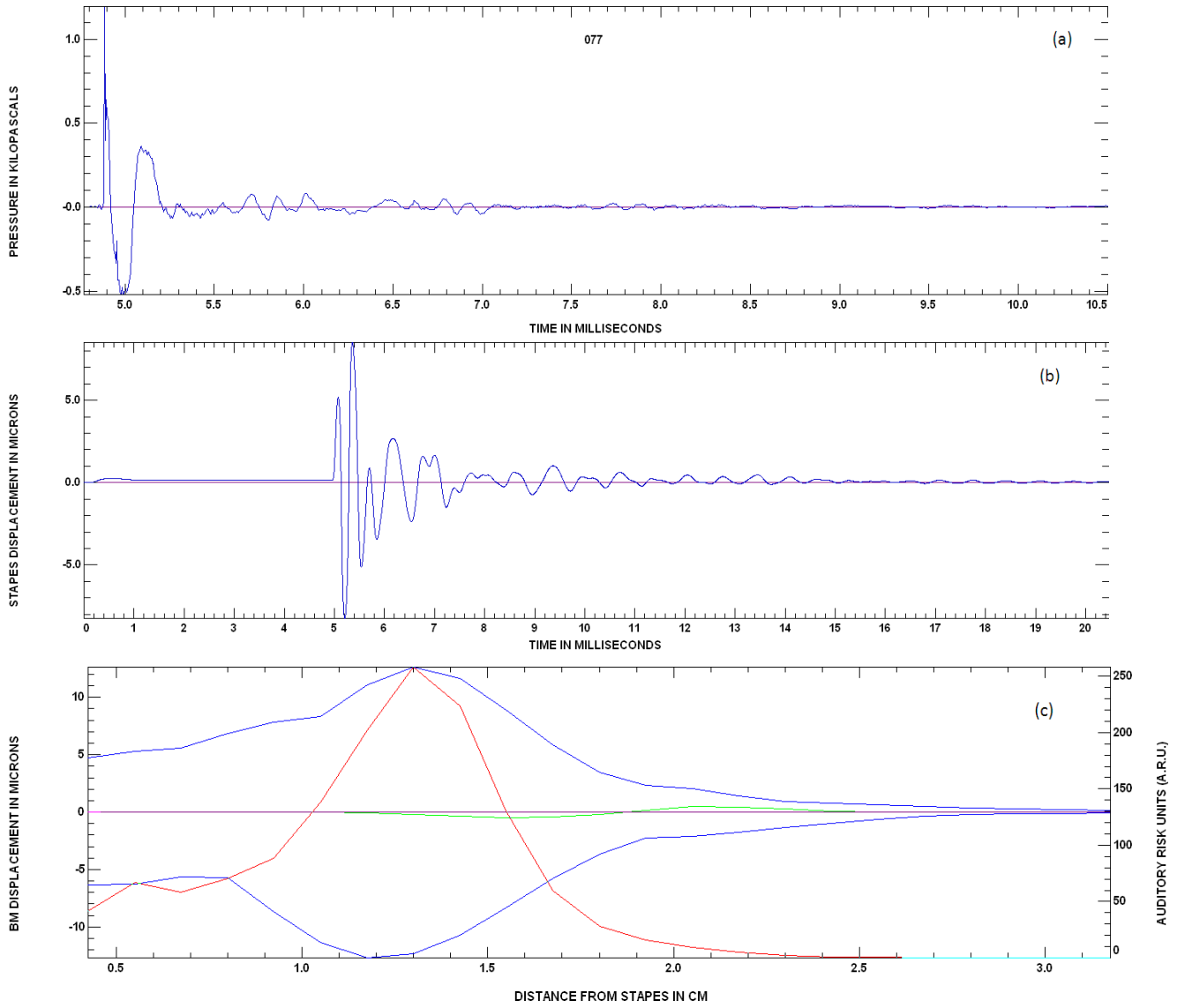

Figure 22 The ARU evaluation of a representative measured impulse noise waveform at SPL = 155 dB: (a) Pressure waveform, (b) the displacement of stapes in human ears, and (c) the BM displacement and ARU change at different distance from the stapes in human ears

ARU vs. voltage of the noise-exposure system

The Figure 23 shows the ARUs produce by measured impulse noises generated from the noise-exposure system. The ARU increases monotonically with the output voltages increasing. In addition, the measured impulse noises generate over 200 ARUs when the output voltages are

greater than 4 v. The results indicate that the impulse noise generated by the noise-exposure system could cause significant hearing loss in animal model.

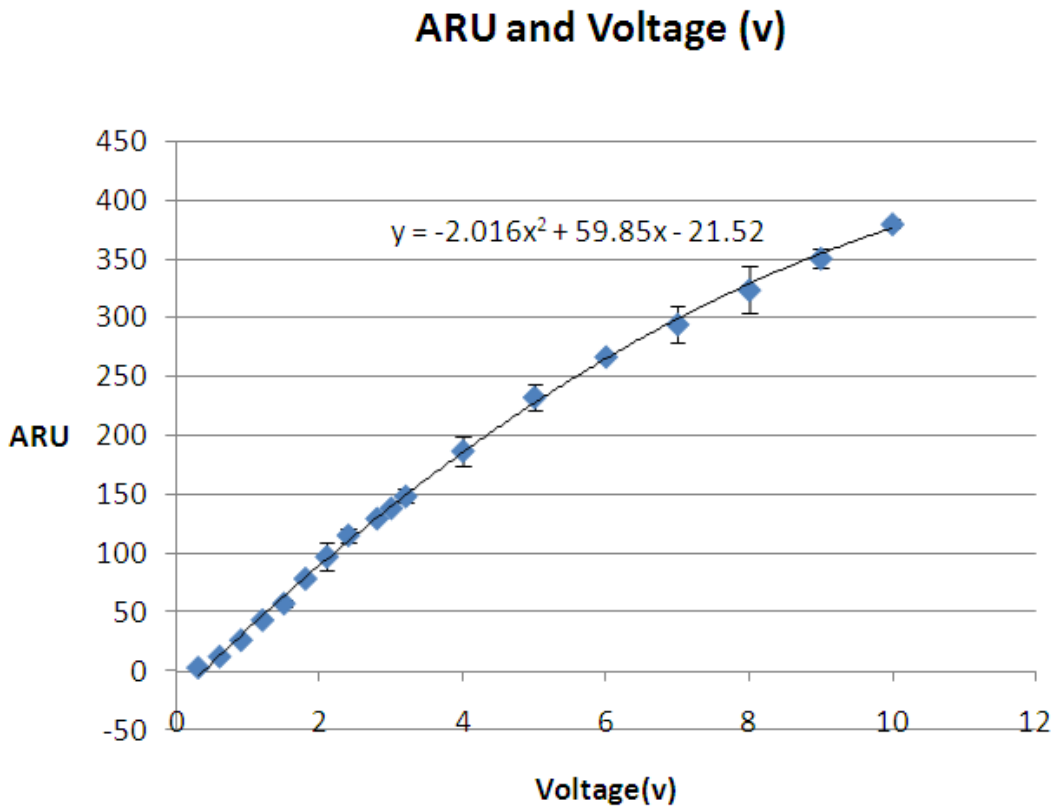

Figure 23 Relationship between ARUs produced by measured impulse noises waveforms and the output voltages of the noise-exposure system.

CHAPTER 6

CONCLUSION

This study focuses on the characteristic analysis for impulse noise in order to estimate acoustic hazardous in NIHL, by using signal analysis method in both time and frequency domain, such as kurtosis as one statistic metric, and together with predicted acoustic hazardous unit, ARU extracted from AHAAH model. Results are evaluated from both simulated sine impulse waveforms and 200 measured impulse noises generated by the noise-exposure system in different voltage control (i.e. 10 data measured at each voltage, in all 20 different voltages). Compared to ARU extracted from test results, AHAAH model is suitable to evaluate impulse noise and is more accurate than the energy based DRC, such as EEH.

According to the results of digital signal analysis on measured impulse noise, FDK analysis demonstrates a uniform tendency in the frequency domain of impulse noises generated by the noise-exposure system at various voltages, meanwhile results from statistic kurtosis analysis in time domain presents that the higher voltage contributes sharper peak of impulse noise. Time duration at negative peak is longer than that at positive peak, which demonstrates a regular impulse noise in terms of time duration. FFT analysis exhibites that the frequency amplitude trends to be raised up as voltage is increasesing. In addition, peak pressure is monotonically increased with voltage amplified. Last but not the least, results from AHAAH model show that ARU is increasing with voltage increasing, meaning more hazardous impulse noises are generated by enhanced voltage from the noise-exposure system.

Based on the simulation results from AHAAH model, the four key parameters of impulse noise play critical roles on auditory hazard prediction. ARUs monotonically increase with the peak pressure (both P^+ and P^-) increasing. Time duration at positive peak produces more auditory hazard than time duration at negative peak in AHAAH model. The results also show that the ARUs are not monotonically increased with time duration rising. The ARUs reach the peak at around t = 0.2 ms and then decrases afterwards. This fact indicates the longer time duration of impulse noise may not lead to a higher auditory hazard. Compared to AHAAH model, EEH principle figures out that the same amount acoustic energy generates identical level of the auditory hazard. Therefore, the accumulated energy in a longer time duration will cause more hearing loss. Typically, positive peak duration of impulse noise is usually less than 0.5 ms. Longer positive time duration may not be considered as impulse noise waveform. Therefore, the AHAAH model may be more accurate than the EEH models for the prediction of auditory hazard from impulse noise.

In addition, the measured impulse noise generated by noise-exposure system could produce large range of ARUs from 0 to 380 as voltage varies. Amplified voltage results in increased ARUs and higher kurtosis (i.e. sharper peak impulse noises), which indicates a higher hearing loss.

CHAPTER 7

DISCUSSION AND FUTURE WORK

Future work is suggested to update the digital signal analysis method, by using the joint time and frequency domain method (i.e. wavelet analysis), with characteristic metrics defined not only for impulse noise but also for compound noise, such as field-measured noise.

In the future work, signal analysis method continues an important role to characterize the impulse noise. Currently, in time domain, kurtosis *K(t)* is introduced to present a sharper-peak impulse noise with voltage increasing. Frequency domain kurtosis (FDK), which is calculated in 1/3-octave filter bank, aims to evaluate the frequency components of impulse noise generated from the noise-exposure system. Furthermore, wavelet analysis will be supplemented to these current methods. In addition, according to the electric human ear principle, the transfer function of human's outer ear and middle ear are functional to be a band-pass filter. Classic mechanical model dominating the process, which is acoustic energy from middle ear into inner ear, is used to derivate the displacement of BM with the parameters of the calculated impedances and sound pressure levels. Since AHAAH software doesn't offer detailed design process and some impedances (Song, 2010), the ARU is simplified by summing of BM displacements' square at location segmented according to 1/3-octave filter bank. In the future, other hearing loss hazard criterions will be investigated.

Four key parameters play important roles in AHAAH model. Results show that in the same time duration, the positive peak pressure generates more ARUs than the negative peak pressure at higher peak pressure level (i.e. $P > 4$ MPa). However, since the field-measured

impulse noise usually has a peak pressure which is ranged from 140 dB to175 dB (about 3 - 4 KPa in peak pressure), there may be no significant difference on the ARUs produced by the positive peak pressure (i.e. the compressive wave) and the negative peak pressure (i.e. the tensile wave). In addtion, field-measured noises are more complex than the simulated sine waves. Therefore, more parameters, such as rise time, are needed to be evaluated in the future work.

Last but not least, future work would be conducted either to improve or to develop a new method to model the human ear's transfer functions with biomedical experiments.

REFERENCES

Agrawal, Y., Platz, E., & Niparko, J. (2008, Jul 28). Prevalence of hearing loss and differences by demographic characteristics among US adults: data from the National Health and Nutrition Examination Survey, 1999-2004. *Arch Intern Med., 168*(14), 1522-1530. doi:10.1001/archinte.168.14.1522.

Alberti, P. (1997). *Pathogenesis of noise-induced hearing loss.* Geneva: WHO-PDH Informal Consultation.

Amrein, B. E. (2010, November 9). *AHAAH: AIBS Review of Impulse Noise Models.* Retrieved 11 1, 2012, from United States Army Research Laboratory: http://www.arl.army.mil/www/default.cfm?page=343

Atherley, & Martin. (1971). Equivalent continuous noise level as a measure of injury from impact and impulse noise. *Ann. Occup. Hyg.*

Auditory and vestibular pathways. (n.d.). Retrieved from http://cnx.org/content/m42297/latest/

Bauer, B. B. (1967). On the Equivalent Circuit of a Plane Wave Confronting an Acoustical Device. *J. Acoust. Soc. Am.*

Bekesy, G. V. (1953). Description of Some Mechanical Properties of the Organ of Corti. *J. Acoust. Soc. Am.*

Binseel, M. S., Kalb, J. T., & Price, G. R. (2009, 9). *Using the Auditory Hazard Assessment Algorithm for Humans (AHAAH) Software Beta Release W93e.* Retrieved 10 1, 2012, from United States Army Research laboratory: http://www.arl.army.mil/arlreports/2009/ARL-TR-4987.pdf

Chan, P. C., Ho, K. H., Kan, K. K., Stuhmiller, J. H., & Mayorga, M. A. (2011, Oct). Evaluation of impulse noise criteria using human volunteer data. *Journal of the acoustical society of Americal, 110*(4), 1967-1975. doi:10.1121/1.1391243

Chan, P. C., Ho, K. H., Stuhmiller, J. H., & Mayorga, M. A. (2001). Evaluation of impulse noise criteria using human volunteer data. *J. Acoust. Soc. Am.*, Volume 110, Issue 4, pp. 1967-1975.

Clark, W. W. (1991). Recent studies of temporary thresholds shift(TTS) and permanent thresholds shift(PTS). *J. Acoust. Soc. Am.* .

D. Tharini, J. P. (2012). 21 Band 1/3-Octave Filter Bank for Digital Hearing Aids. *Proceedings of the Internal Conference on Pattern Recognition, Informatics and Medical Engineering.* IEEE.

Daniel, E. (2007, May). Noise and Hearing Loss: A Review. *Journal of School Health, 77*(5), 225-231. doi:10.1111/j.1746-1561.2007.00197.x

Dewey, J. M. (2004). The shape of the blast wave: studies of the friedlander equation. *EJSE International*.

Dwyer, R. F. (1984). Use of the Kurtosis Statistic in the Frequency Domain as an Aid in Detecting Random Signals. *IEEE*.

Erdreich, J. (April 1986). A distribution based on definition of impulse noise. *J. Acoust. Soc. Am.*, 79(4).

Gardner, M. B., & Hawley, M. S. (1972). Network Representation of the External Ear. *J. Acoust. Soc. Am*, 52.

Givelberg, E., & Bunn, J. (2003). A comprehensive three-dimensional model of the cochlea. *J. of Computational Phy.*

Guinan, J. J., & Peake, W. T. (1967). Middle-Ear Characteristics of Anesthetized Cats. *J. Acoust. Soc. Am.*, Volume 41, Issue 5, pp. 1237-1261.

Hearing. (2012). Retrieved from Connections: http://www.bioon.com/bioline/neurosci/course/audvest.html

ISO. (1990-01-15). *Acoustics-Determination of occupational noise exposure and estimation of noise-induced hearing impairment.* ISO 1999.

Johnston, A. M. (2011). *Noise exposure system for noise induced hearing loss.* Department of Biomedical Engineering. Carbondale, IL: Southern Illinois University Carbondale.

Johnston, M. A. (2011). *Noise exposure system for noise induced hearing loss.* Thesis, Southern Illinois University Carbondale, Department of Biomedical Engineering, Carbondale, IL. Retrieved from http://vufind.carli.illinois.edu.proxy.lib.siu.edu/all/vf-sic/Record/12985908/Request

Kardous, C. A., Willson, R. D., & Murphy, W. J. (2005). Noise dosimeter for monitoring exposure to impulse noise. *Applied Acoustics*, 974-985.

Levey, S., Fligor, B. J., Ginocchi, C., & Kagimbi, L. (2012). The Effects of Noise-Induced Hearing Loss on Children and Young Adults. *Contemporary Issues in Communication Science and Disorders*.

Murphy, W. J., & Kardous, C. A. (2012). *A case for using A-weighted equivalent energy as a damage risk criterion.* EPHB 350-11a.

Pfander, Fongartz, & Brinkmann. (1980). Danger of auditory impairment from impulse noise: A comparative study of the CHABA damage-risk criteria and those of the Federal Republic of Germany. *J. Acoust.Soc. Am.*

Price, G. R. (1965). Middle-Ear-Muscle Effects on Low-Intensity Sounds. *J. Acoust. Soc. Am.*, Volume 38, Issue 5, pp. 918-918.

Price, G. R. (1985). Mechanisms of loss for intense sound exposures. In R. R. Fay, G. Gourevitch, Editor, & L. Kitzes, *Hearing and Other Senses: Presentations in Honor of E. G. Wever* (p. 337). J. Acoust. Soc. Am.

Price, G. R. (1991). Middle ear muscle effects during gunfire noise exposures. *J. Acoust. Soc. Am.*, Volume 89, Issue 4B, pp. 1865-1865.

Price, G. R. (2007). Validation of the auditory hazard assessment algorithm for the human with impulse noise data. *J. Acoust. Soc. Am.*, Volume 122, Issue 5, pp. 2786-2802.

Price, G. R. (2010). *Impulse noise and the cat cochlea.* MD: U.S. Army Research Laboratory.

Price, G. R., & Kalb, J. T. (1986). Mathematical model of the effect of limited stapes displacement on hazard from intense sounds. *J. Acoust. Soc. Am.*, Volume 80, Issue S1, pp. S123-S123.

Price, G. R., & Kalb, J. T. (1991). Insights into hazard from intense impulses from a mathematical model of the ear. *J. Acoust. Soc. Am.*, Volume 90, Issue 1, pp. 219-227.

Price, G. R., & Wansack, S. (December 1989). Hazard from an intense midrange impulse. *J. Acoust. Soc. Am.*, 86(6).

Roberto, M., Hamernik, R. P., Salvi, R. J., Henderson, D., & Milone, R. (1984). Impact noise and the equal energy hypothesis. *J. Acoust. Soc. Am.*

Sense of Hearing. (n.d.). Retrieved from Human Anatomy: http://encyclopedia.lubopitko-bg.com/Sense_of_Hearing.html

Smoorenburg, F. G. (1983). Damage risk criteria for impulse noise. *New perspectives on Noise-induced Hearing Loss*.

Song, W. J. (2010). *Study on Human Auditory System Models and Risk Assessment of Noise Induced Hearing Loss.* Cincinnati: University of Cincinnati.

Stevin, G. O. (Dec. 1982). Spectral analysis of impulse noise for hearing conservation purpose. *J. Acoust. Soc. Am. 72(6).*

U.S. Department of Labor. (n.d.). Retrieved from Occupational Safety & Health Administration: https://www.osha.gov/pls/oshaweb/owadisp.show_document?p_table=STANDARDS&p_id=9736

Wang, H., & Chen, P. (Oct. 2009). Fault Diagnosis Method Based on Kurtosis Wave and Information Divergence for Rolling Element Bearings. *Wseas Transactions on Systems*.

Wu, Q., & Qin, J. (2012). Effects of Key Parameters of Impulse Noise on Prediction of the Auditory Hazard Using AHAAH Model. *International Journal of Functional Informatics and Personalized Medicine*.

Zhu, X., Kim, J. H., & Song, W. J. (2009). Development of a noise metric for assessment of exposure risk to complex noises. *J. Acoust. Soc. Am.*

VITA

Graduate School
Southern Illinois University

Qing Wu

lauraqing.wu@gmail.com

Southwest University of Science & Technology (SWUST)
Bachelor of Science, Mechanical Engineering, June 2006

Florida International University (FIU)
Master of Science, Electrical Engineering, April 2008

Beihang University
Master of Science, Software Engineering, July 2009

Special Honors and Awards:

- Academic Awards:
  - Won "Outstanding Thesis Award", SWUST, July 2006
  - Won "Academic Excellence Award", SWUST, 25th. Nov. 2005
  - Won the title of "First Class Scholarship", SWUST, 28th. Nov. 2003
- Association/Activities Awards:
  - Won "Excellence Award" in National College Theatre Festival, Chengdu, Aug. 2005
  - Vice president of College Students Image Strategy & Design Association, SWUST, 2004-2005
  - Promotion officer of Study Department of the Student Union, SWUST, 2002-2003

Thesis Title:

Characterization of Impulse Noise and Hazard Analysis of Impulse Noise Induced Hearing Loss using AHAAH Modeling

Major Professor: Dr. Jun Qin

Publications:

Qing Wu, Jun Qin, “Effects of Key Parameters of Impulse Noise on Prediction of the Auditory Hazard Using AHAAH Model,” International Journal of Functional Informatics and Personalized Medicine, 2012.

Qing Wu, Zhang Jin, “The Algorithm VLD Optimization based on CABAC decoder and its logic realization”, Beihang University Master's Thesis, in Ingenic Semiconductor Co. Ltd., 2007